CHAPTER III

RESULTS AND DISCUSSION

3.1 Design Concept

It is known that tetraethylene glycol dimethyl ether (glyme), polyethylene glycol and their ethers are one of the most versatile building blocks suitable for attaching receptors or sensory units on both of their terminals. Binding with metal compels the conformation change which influence on appended receptors or signaling units that placed at both terminals of podand. Therefore, these systems are of considerable interest because of their useful applications in molecular switches, molecular sensors, molecular gates, and etc.[9-12]

On the basic of this strategy, we placed urea or thiourea moieties at both of terminals of podand. That expected for making in bifunctional receptors or/and allosteric switches. We have been intrigued by the utilization of highly flexible acyclic crown ether, the large structural change from linear crown ether to pseudocyclic crown ether upon complexation with an alkali metal ion. According to the desired property, suitable urea or thiourea moieties should be preorganized in the system for binding anion via hydrogen bonding.

Thus, ligands **5a**, **5b** and **5c** were synthesized by attaching hexyl urea moieties, *p*-nitrophenyl thiourea moities and phenyl urea moieties, respectively at both terminals of the podand and studied complexation by ^{1}H-NMR titration for the case of ligand **5a**. Ligand **5b**, containing *p*-nitrophenyl thiourea moieties as a chromophore, was designed for studying complexation by UV-vis technique. We expected that ligand **5b** would show a naked sensing ability. The synthetic pathway is shown in Scheme 1.

3.2 Synthesis and characterization of acyclic crown ether derivatives containing urea/thiourea moieties

3.2.1 Synthesis and characterization of *o*-methoxy phenol (1a)

Phenol groups are very versatile functional groups for the synthesis of various compounds. We have recently conversed pyrocatechole to *o*-methoxy phenol by using a simple nucleophilic substitution reaction. The commercial pyrocatechol was reacted

with iodomethane (1 equiv.) in the presence of anhydrous potassium carbonate as based in dried acetronitrile yielding *o*-methoxy phenol as yellowish oil in 85% yield after purification by silica gel column chromatography using dichloromethane as eluent. The ^{1}H-NMR spectrum of **1a** showed singlet peak of the methoxy protons and broad peak of the phenolic hydroxy proton at 3.87 and 5.70 ppm, respectively, with an integral ratio of 3:1. It is thus in good agreement with the proposed structure.

3.2.2 Synthesis and characterization of 2-methoxy-6-nitrophenol (2a) and 2-methoxy-4-nitrophenol (2b)

The synthesis of 2-methoxy-4-nitrophenol **2b** started with electrophilic substitution of *o*-methoxy phenol. A mild condition was used for generating nitronium ion in order to prevent oxidation of the phenol group.

In this case, the reaction was carried out by addition of a solution of nitric acid in to a mixture of *o*-methoxy phenol **1a** and glacial acetic acid in acetonitrile resulting in only 8 % yield of by product, 2-methoxy-6-nitrophenol **2a**, and 46% yield of 2-methoxy-4-nitrophenol **2b**. Consequently, the hydroxy group is a stronger activating group on the stability of intermediate than the methoxy group, which influence on the stability of arenium ion intermediate at the para position more than the ortho and the meta positions.[46]

The ^{1}H-NMR spectrum of **2a** showed a singlet downfield signal of the hydroxy proton at 10.75 ppm due to the intramolecular hydrogen bonding between nitro group and the adjacent of hydroxy group (ortho position). The aromatic protons and the methoxy protons appeared at 7.69-6.92 and 3.92, respectively, which shifted more down fields than **1a**.

In the case of **2b**, the hydroxy group was in the para position with respect to the nitro group. Thus, the ^{1}H-NMR spectrum showed the signal of hydroxy proton at 6.22 ppm which was not able to form intramolecular hydrogen bonding with the opposite side of the nitro group. The aromatic protons and the methoxy protons exhibited the same pattern as that of compound **2b** which signals appeared at 7.93-7.03 ppm and 4.04 ppm, respectively. EI mass spectra also supported the structure of this compound showing an intense line at m/z 169 and elemental analysis was in good agreement with the proposed structure.

3.2.3 Synthesis and characterization of 3a

The synthesis of the compound **3a** was to couple a unit of podand with 2-methoxy-4-nitrophenol **2b** together. One unit must have a good leaving group such as toluenesulfonyl (TOS), Br and I. By using this strategy, we transformed two hydroxy groups of tetraethylene glycol to tetraethylene glycol ditosylate and then coupling with 2-methoxy-4nitrophenol **2b** that had a stable protonation form of aryloxide ion, which acted as a good nucleophile because of the para-detecting of nitro group.

The synthetic pathway started with a preparation of trtraethylene glycol ditosylate by tosylation of tetraethylene glycol in the presence of 3 equiv. of triethylamine and a catalyst amount of DMAP in dichloromethane at room temperature overnight. After purification by column chromatography using dichloromethane as eluent, a colorless oil of tetraethylene glycol ditosylate showed the characteristic peaks of tosyl groups: siglet of the methyl proton (ArCH_3) at 2.39 ppm, two doublets of the aromatic protons (ArH) at 7.73 and 7.30 ppm and the bridging glycolic protons (OCH_2CH_2O) appeared at 4.10-3.54 ppm. They are accordance with the structure of tetraethylene glycol ditosylate.

The coupling reaction of tetraethylene glycol ditosylate with 2-methoxy-4-nitrophenol **2b** in acetonitrile using 10 equiv. of anhydrous potassium carbonate as based afforded 2,2′-[oxabis(4-oxapentaethlenoxy)-bis(2-methoxy-4-nitrophenol)] **3a** as a yellowish crystalline solid in 85% yield after recrystallization with methanol.

The ^{1}H-NMR spectrum of **3a** showed absence of two doublets aromatic protons at 7.73 and 7.30 ppm of the tetraethylene glycol and two doublets and one doublet of doublet of the aromatic protons of 2-methoxy-4-nitrophenol moieties were found at 7.91-6.98 ppm instead. Moreover, the methoxy protons and the bridging glycolic protons appeared at 3.96 and 4.31-3.71 ppm. EI mass spectra also supported the structure of this compound showing an intense line at 496 m/z, which correspond to the result of elemental analysis.

3.2.4 Synthesis and characterization of 4a

The reduction of nitro compounds to amine is very useful synthetic transformation. In this case, we searched for a mind condition, selective reduction to nitro groups, inexpensive reagents, a high yielding and a general method for this transformation. Hydrazine and a hydrogenation catalyst have been selected for the reduction of the nitro substitutions of **3a**. The reaction was carried out by addition of

hydrazine into a mixture of **3a** in the presence of Raney nickel in a mixed solvent of methanol/ethyl acetate to give yellow oil of **4a** in quantitative yield.

The compound showed a very broad signal in ^{1}H-NMR spectrum at 3.90 ppm corresponding to the amine protons. Higher upfield shifts of the aromatic protons of the compound compared to aromatic protons of compound **3a** were increased due to the shielding effect of the amine groups.

3.2.5 Synthesis and characterization of *p*-nitrophenyl thioisocyanate

One of the most common methods for the preparation of thioisocyanate is to react thiophosgene with primary amines to give chlorothioformamide (ClCSNHR) that lose of HCl to obtain thiocyanate (RNCS). In this case, the preparation of *p*-nitrophenyl thioisocyanate was carried out by stirring a mixture of *p*-nitroaniline with thiophosgene in CH_2Cl_2 at room temperature. Sodium hydrogencarbonate were added into the mixture for trapping HCl that evolved from the reaction. After recrystallization with methanol, a bright yellow crystalline solid was obtained in 93% yield. The ^{1}H-NMR spectrum of *p*-nitrophenyl thiocyanate showed the characteristic peaks of the compound which were in good agreement with the literature.[45]

3.2.6 Synthesis and characterization of 5a, 5b and 5c

The final products (ligands **5a** and **5c)** were obtained by reacting compound **4a** with *n*-hexyl isocyanate and phenyl isocyanate in CH_2Cl_2 under nitrogen atmosphere. Ligands **5a** and **5c** were obtained as white powder in 68% yield and 90% yield, respectively. The compound **4a** was then altered to the final product (ligand **5c**) by coupling with *p*-nitrophenyl thioisocyanate resulting in a bright yellow crystalline of **5c** in 46% yield.

^{1}H-NMR spectrum of **5a, 5b** and **5c** showed the absence of broad signals due to the amine proton at 3.90 ppm and the signals of the urea-NH protons were found instead at 6.58 and 5.01 ppm, 10.19 and 10.10 ppm and 7.58 and 7.28 ppm, respectively. Mass spectra also supported the structure of the ligands **5a** and **5b** showing signals at m/z 691.4 and 797.2. The elemental analysis result also agreed with the purposed structure of **5a**.

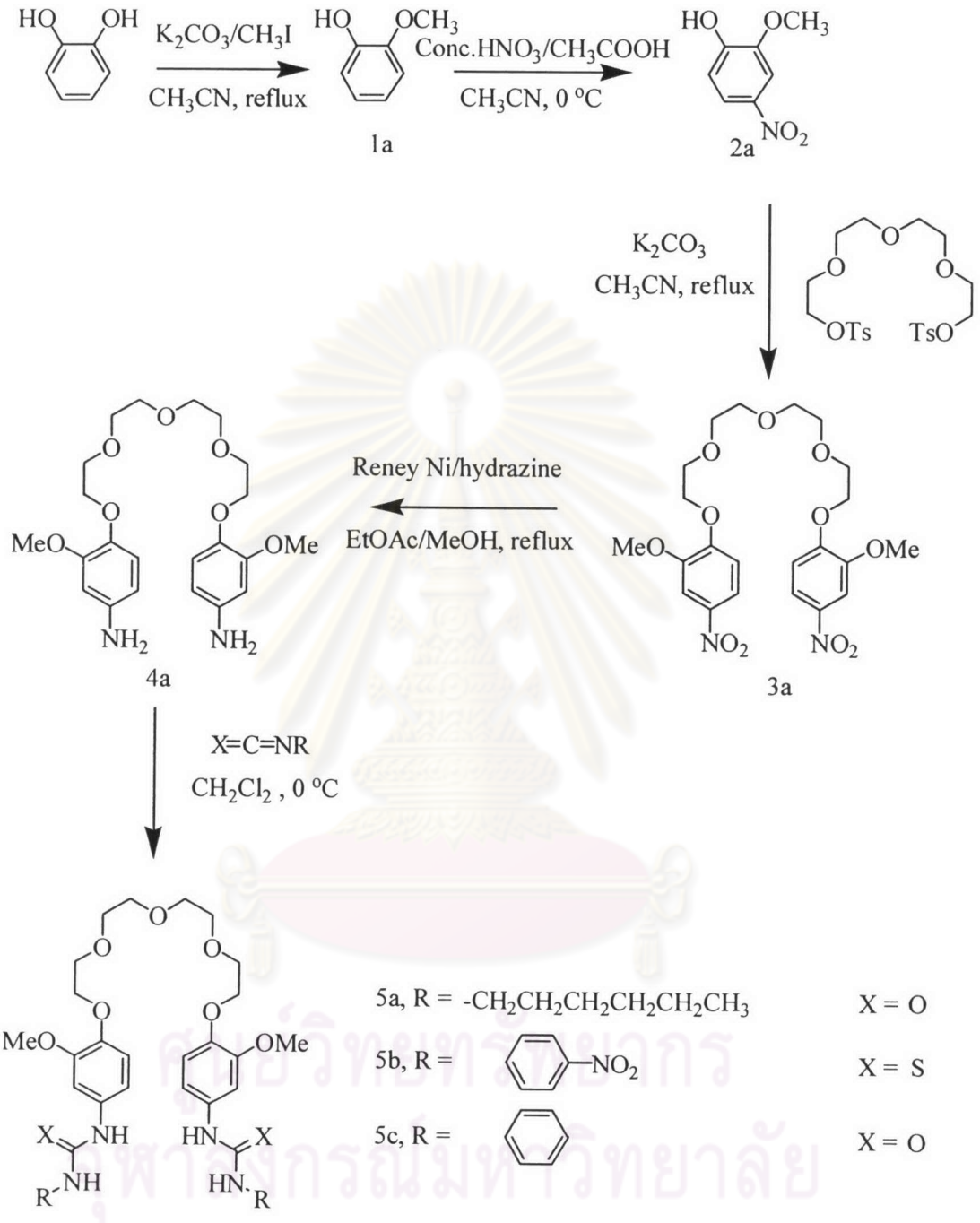

Scheme 1 The synthetic pathway of all final products **5a**, **5b** and **5c**

3.3 The complexation studies of ligand 5a by using ^{1}H-NMR titrations

3.3.1 Cation complxation studies

Ligand **5a** contains ethylene glycol linkages, which have oxygen donor atoms for binding alkaline metal ions like crown ether. Thus, complexation studies of ligand **5a** with alkaline metal ions such as Na^+ and K^+ were investigated for searching the best of alkaline metal ions that were able to bind with ligand **5a** for studying the effect of the structural change and the effect of Na^+ toward anion binding ability (as described below in section **3.3.3**)

^{1}H-NMR titration studies were carried out in the absence and presence of metal ions. Peak assignments were made by ^{1}H-H COSY and NOESY spectra, showed in Figure 3.1. ^{1}H-NMR spectra provided information on the structure of the metal complexes. The chemical shifts of ligand **5a** and their induced chemical shifts on the formation of complexes with Na^+ and K^+ ion are listed in Table 3.1.

Table 3.1 Chemical shifts (ppm) of ligand **5a** and their changes at complexation with various cation complexes.*

	H_a	H_b	H_c	b1	b2	b3	OMe	K(M^{-1})**
ligand **5a**	7.03	6.70	6.50	3.64	3.80	4.05	3.73	-
5a.Na^+	-0.35	-0.22	-0.02	-0.10	-0.19	-0.21	-0.13	443
5a.K^+	-0.35	-0.08	0.10	-0.13	-0.15	-0.16	-0.37	88

* Positive value showed downfield shifts and negative value showed upfield shifts. All spectra were recorded on a Bruker DRX 400 MHz nuclear magnetic resonance spectrometers.

** Association constants are the average of all ligand **5a**, which exhibited significant complexation induced shifts (uncertainly 10%)

The Job's plots of **5a.Na**$^+$ and **5a.K**$^+$ are symmetric and show a maximum the mole fraction of guest at 0.5, which indicated a 1:1 guest-host stoichiometry as shown in Figure 3.2. The association constants with alkali metal ions have been determined by using EQNMR program[47] and are summarized in Table 3.1.

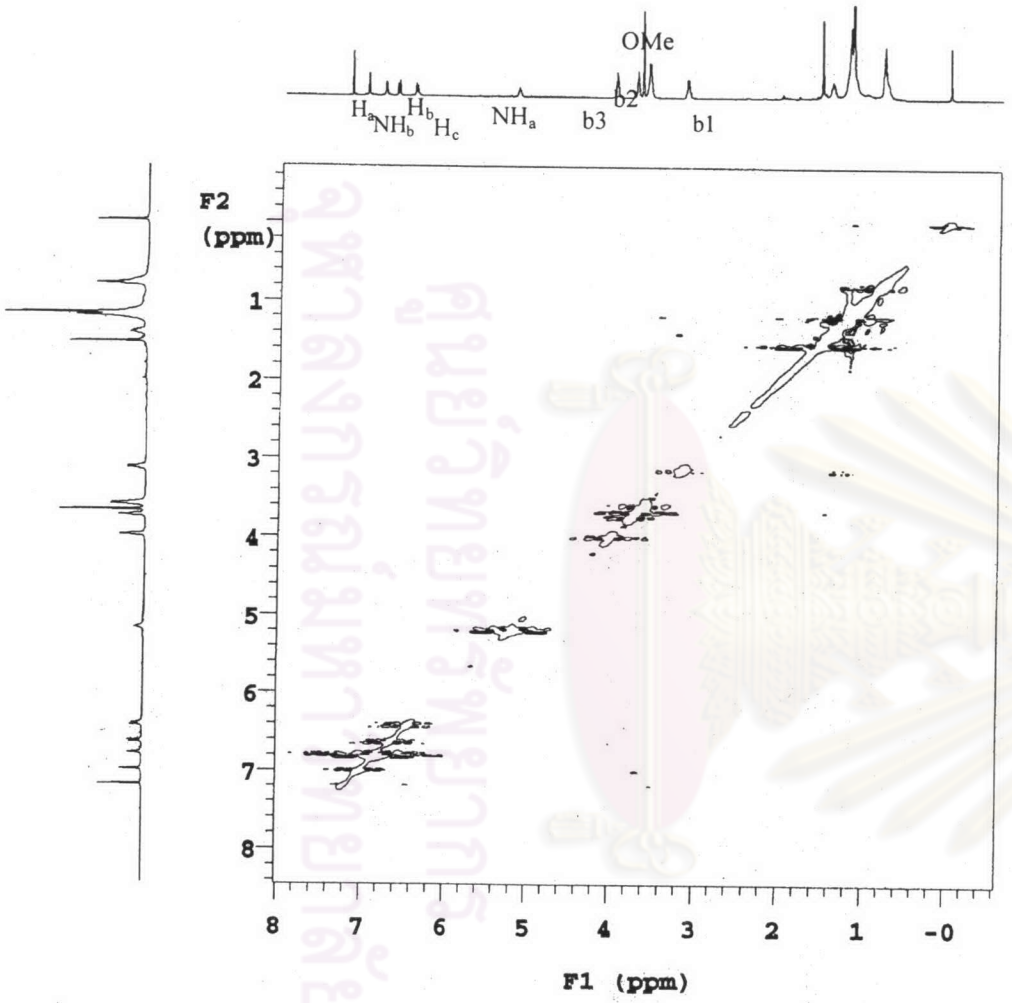

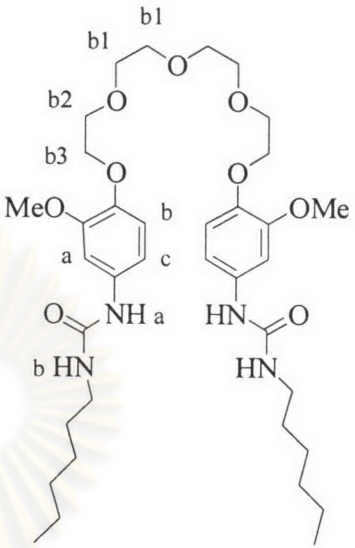

Figure 3.1 ^{1}H-H COSY of ligand **5a**

In the case of Na^+, all of the oxyethylene bridge protons and the methoxy protons showed slightly upfield shifts (b1, $\Delta\delta = 0.10$; b2, $\Delta\delta = 0.19$; b3, $\Delta\delta = 0.21$ and OMe, $\Delta\delta = 0.13$ ppm, respectively). The upfield shifts should be due to the aromatic ring current. These results indicated that Na^+ bind oxygen atoms of the methoxy moieties and the tetraethylene glycol unit. On the other hand, high magnetic field shifts of the phenyl protons (H_a-H_c, $\Delta\delta =$ 0.02-0.35 ppm) can be explained by shielding due to stacking of the phenyl rings. This confirmed by the overlapping between the aromatic protons H_b and H_c upon addition of 1 equivalent of $NaClO_4$. Hence, the ^{1}H-NMR data observations also reflect a large conformation changed of **5a** from non cyclic crown ether to pseudocyclic crown ether inducing during complexation with Na^+.

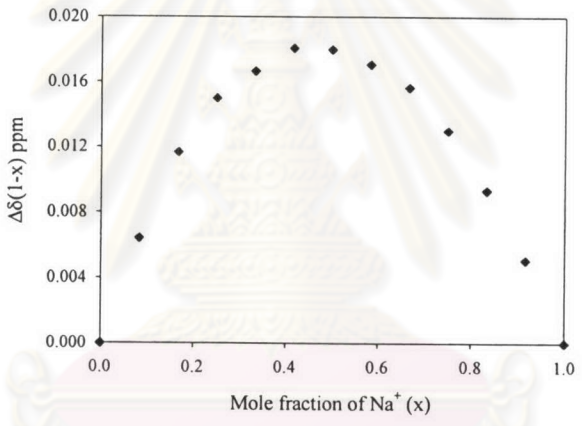

Figure 3.2 Job's plot of the complexation of **5a**.Na^+ on the chemical shift of an oxyethylene bridge.

In the ^{1}H-NMR data, **5a**.K^+ complex had a smaller upfield shift of protons on the oxyethylene bridges b2-b3 than the complex of **5a**.Na^+, $\Delta\delta = 0.13$, $\Delta\delta = 0.15$ and $\Delta\delta = 0.16$ ppm, respectively. Although the methoxy protons exhibited significant high magnetic field shift $\Delta\delta =$ 0.37 ppm. The aromatic proton H_b did not merge with aromatic proton H_c during addition of 1 equivalent of K^+. This reflects the weak $\pi-\pi$ interactions between aromatic rings because the ionic radius of K^+ is probably too large and not suitable for the glyme-5 moiety. This fact corresponds to the complex formation constant for Na^+ that is 5 times higher than that of K^+.

In summary, the preference for Na^+ suggested that cavity of pseudocyclic formed was more complementary to the size of the Na^+ than to K^+ ion. Apparently, this better fit dominates the expected higher bonding of hard Na^+ ion for hard oxygen atoms. Finally, these results lead us to propose the structure of complexation between ligand **5a** with Na^+ as shown in Figure 3.3.

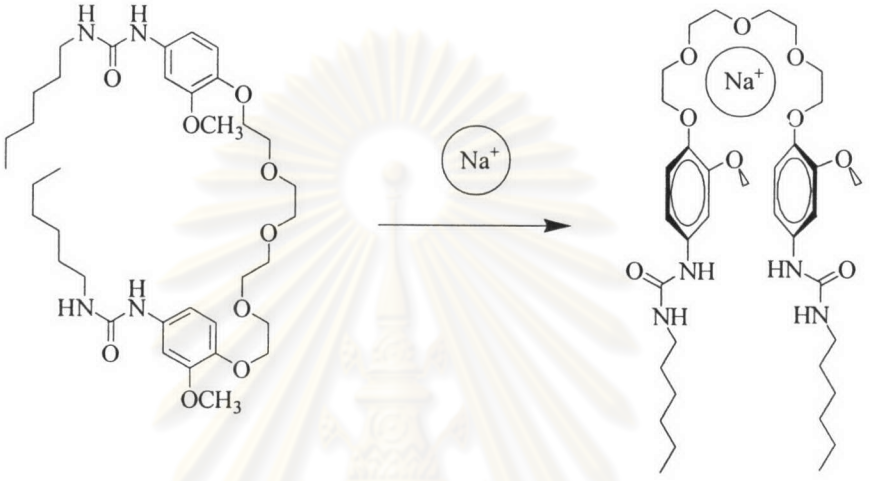

Figure 3.3 Structural change of **5a** induced by Na^+

ศูนย์วิทยทรัพยากร
จุฬาลงกรณ์มหาวิทยาลัย

3.3.2 Anion complexation studies

Ligand **5a** also contains four urea NH groups designed as an anion binding site via hydrogen bonding interactions. Association constants toward various size and geometry of anions were determined for deducing the relationship between anion properties and anion binding abilities of the ligand **5a**.

In ^{1}H-NMR titration experiments of the ligand **5a** with $Bu_4N^+A^-$ in chloroform-d, the signals of NH_a and NH_b of the ligand **5a** shifted to downfield ($\Delta\delta$ ~1–3 ppm) upon addition of 0.1-4 equivalents of tetrabutylamonium anions. Also, small downfield shifts for the protons of phenyl rings were observed, which may be attributed to increased electron density in phenyl rings due to the presence of anions.

Induced chemical shift changes of ligand **5a** on the formation of complexes with various anions were listed in Table 3.2

Table 3.2 The chemical shifts ($\Delta\delta$ ppm) of NH protons and association constants of ligand **5a** toward various anions*

Anion	NH_a	NH_b	K (M^{-1})**
Chloride	1.43	1.78	498
Bromide	1.10	1.63	459
Iodide	0.79	1.13	164
Nitrate	1.26	1.61	672
Acetate	1.85	2.73	778
Benzoate	2.38	3.05	658
Dihydrogenohosphate	2.53	2.82	1188

* Positive value showed downfield shifts and negative value showed upfield shifts. All spectra were recorded on a Varian 400 MHz nuclear magnetic resonance spectrometers.

** Association constants are the average of all ligand **5a,** which exhibited significant complexation induced shifts (uncertainly 10%)

Probably the formation of the complexes are in details, before the formation of the complex, phenyl protons H_b and H_c were separated at 6.66 and 6.44 ppm, respectively. This result suggested that ligand **5a** formed an unfolding structure and no intramolecular π–π interactions of two phenyl rings.

After addition of anions, the phenyl proton H_b showed downfield shifts and overlapped with the phenyl proton H_c that inferred stacking of the two phenyl rings. Hence, a conformation change of ligand **5a** was induced during complexation of an anion via hydrogen bonding with the aid of intramolecular $\pi-\pi$ interactions.

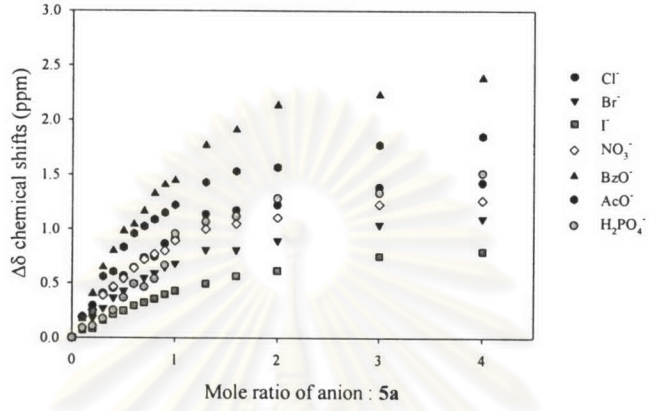

Figure 3.4 The ^{1}H-NMR titration curves of **5a** towards various anion ratios in $CDCl_3$ versus chemical shifts of a NH proton.

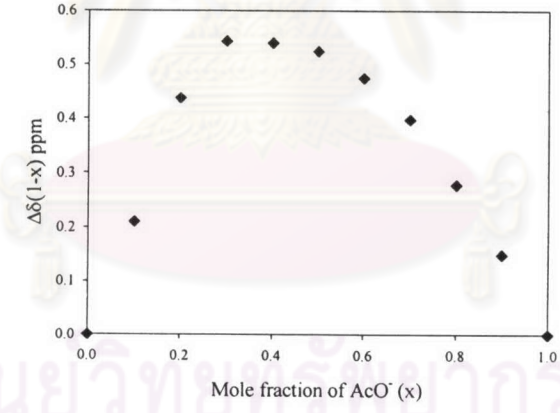

Figure 3.5 Job's plot of the complexation of **5a**.AcO^- on chemical shifts of the NH_a proton.

^{1}H-NMR titration curves of ligand **5a** toward various anions are depicted in Figure 3.4. In all cases, the stoichiometry is 1:1 as confirmed by Job's plots (See for an example in Figure 3.5). On the basis of ^{1}H NMR data, an expected structure of anion complexes with ligand **5a** before and after the addition of anion is depicted in Figure 3.6.

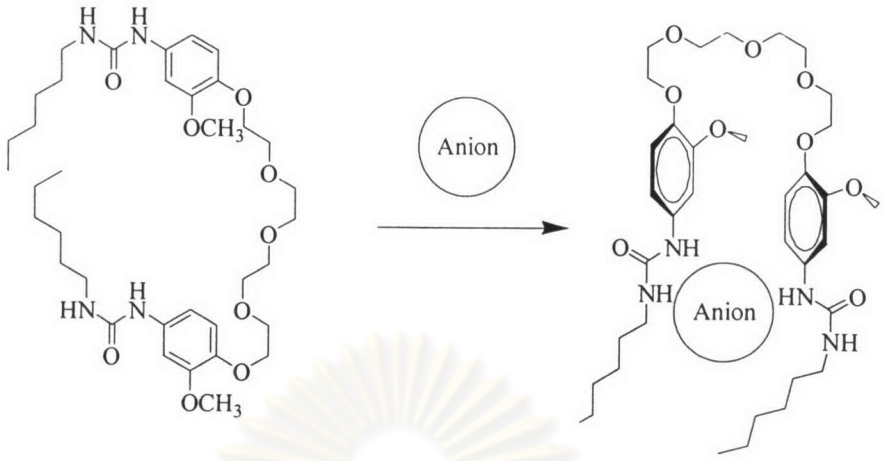

Figure 3.6 Structural change of **5a** induced by an anion

Nevertheless, ligand **5a** with the flexible linker, poly(oxyethelene) bridge unit, may probably be adopted a 2:2 linear anion complexation inducing by intermolecular π–π interactions as shown in Figure 3.7. The association constants with various anions have been determined by using the EQNMR program and are summarized in Table 3.2.

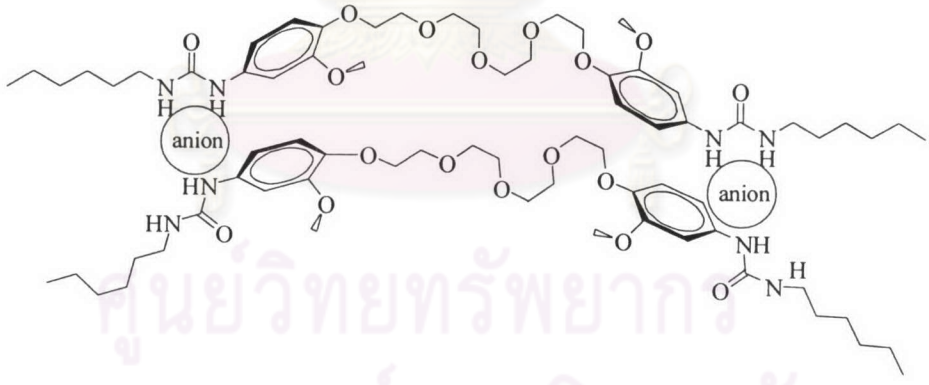

Figure 3.7 The structure of an anion complex in a 2:2 linear complexation

The host **5a** showed a preference for anions in the order of dihydrogenphosphate > acetate > nitrate ~ benzoate > chloride > bromide > iodide. In spite of the less basic character of $H_2PO_4^-$ (pKa = 2.12) compared to AcO^- (pKa = 4.76), $H_2PO_4^-$ showed stronger binding affinity to ligand **5a** than acetate. The binding tendency of ligand **5a** for anions is similar to that of acyclic or cyclic bis-ureas.[20-22,48] Thus, ligand **5a** prefers to bind an anion in the tetragedral geometry. Furthermore,

$H_2PO_4^-$ with four oxygens makes a strongest complex via multitopic hydrogen bonding interactions with ligand **5a**.

In the case of AcO^-, NO_3^- and BzO^-, they have trigonal planar geometry. The association constants can be understood on the basic of the anion basicity and binding sites of anions. According to the basicity of anions, AcO^- exhibits a higher affinity than BzO^- and NO_3^-. However, NO_3^- is less basic (pK_a = -1.64) than BzO^- (pK_a = 4.20). Nevertheless, it has almost the same binding value as BzO^- because of multitopic hydrogen bonding of NO_3^-.

Moreover, we investigated the anion binding affanities toward spherical anions resulting in significant complexation of Cl^-, Br^- and weak complexation of I^-. This can be explained by the anion basicity and the hard-solf acid-base between anions and hard urea protons.

In conclusion, the selectivity is governed by geometry and binding site of anions for hydrogen bonding interactions with ligand **5a** rather than anion basicity. It should be noted that the flexible podand spacer containing bis-urea, ligand **5a**, showed lower association constants when compared to rigid spacers like xanthene[20,48] linking the two urea groups due to a highly preoganized structure. However, this molecule contained the polyethylene glycol unit for the binding site with alkali metal ions that may induce a conformation change into a preorganized structure for binding anions by a metal template.

ศูนย์วิทยทรัพยากร
จุฬาลงกรณ์มหาวิทยาลัย

3.3.3 Complexation studies of ligand 5a in the presence of 2 equivalents of $NaClO_4$ toward various anions such as chloride, bromide, iodide, nitrate, acetate, benzoate and dihydrogenphosphate

Ligand **5a** has selectivity toward Na^+ and its complexation has ability to organize the flexible ligand into a rigid and preorganized structure of urea moieties for binding anion by a metal templated effect. Thus, in this section we would to investigate the effect of Na^+ on anion binding ability of ligand **5a**. ^{1}H-NMR titration experiments were carried out repeatedly in the presence of 2 equivalents of $NaClO_4$, performed complex **5a**.Na^+. The association constants in this system with various anions are collected in Table 3.3.

Table 3.3 Comparison of anion complexation constants between the systems of free ligand **5a** and **5a**.Na^+ with various anions

	K (M^{-1})*	
Anion	**5a**	**5a**.Na^+
Chloride	498	a
Bromide	459	a
Iodide	164	342
Nitrate	672	a
Acetate	778	a
Benzoate	658	a
Dihydrogenphosphate	1188	312

* Association constants are the average of all ligand **5a**, which exhibited significant complexation induced shifts (uncertainly 10%)

[a] Association constants could not be determined due to the ion pairing effect.

In the case of I^-, addition of Bu_4NI to a solution of the **5a**.Na^+ complex results in a clear downfield shift of the NH signals that produce a "normal looking" titration curves as shown in Figure 3.8. Analysis of the resulting titration curve with the computer program EQNMR suggested a 1:1 complex stoichiometry with the stability constant of 312 M^{-1} (see Table 3.3), which increased approximately 1.6 folds higher than that in the absence of Na^+. The result indicated the Na^+ induced a positive cooperativity of I^- binding. This might be a consequence of favorable electrostatic

attractions between the pseudocyclic crown ether bound Na^+ and urea complexed anion. The purposed structure of this complexation is shown in Figure 3.9.

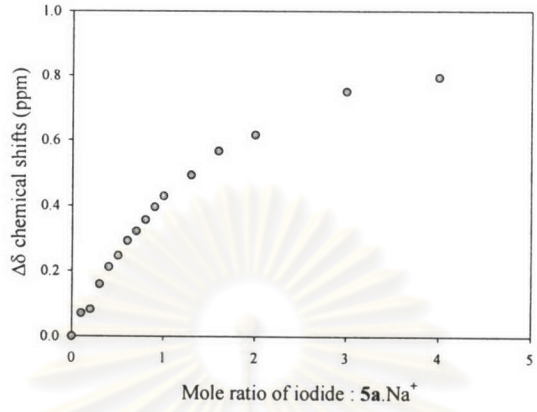

Figure 3.8 The ^{1}H-NMR titration curve of **5a**.Na^+ towards iodide anion in $CDCl_3$ on the chemical shifts of NH proton

In contrast to the case of $H_2PO_4^-$, the calculated association constant was decreased from 1188 to 342 M^{-1} by the presence of 2 equivalents of sodium perchlorate. Interestingly, the stability constant was less than expected. This is probable to introduce that Na^+ functioned as a co-bound $H_2PO_4^-$ to form ion pair which withdraw electron density and decreased basicity of $H_2PO_4^-$.

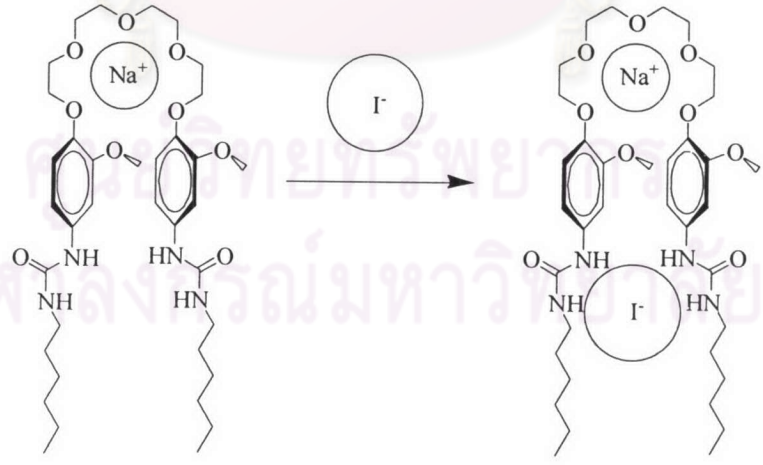

Figure 3.9 The purposed complex structure of **5a.Na**$^+$ with iodide ion

In a similar fashion, addition of 1 equiv. of Br^-, 1.3 equiv. of NO_3^-, 2 equiv. of Cl^- and BzO^-, and 3 equiv. AcO^- showed no significant shift of the resonance corresponding to both NH protons, which generated the data that could not be fit to any binding models. Apparently, Na^+ in these systems possibly inhibited the anion affinities which prevent host/anion binding by the ion pairing effect.

However, as the experiment progress and more equivalents of the above anions were added to the solution. The anion binding site seems to be reactivated, as observed by the sudden downfield shift of the NH signals. Clearly the hydrogen-bonding recognition site for anions was reconstructed in response to the excess anionic species. A clear example is presented by the ^{1}H-NMR titration curve of **5a**.Na^+ with Br^- in the presence of 2 equivalents sodium perchlorate as shown in Figure 3.10.

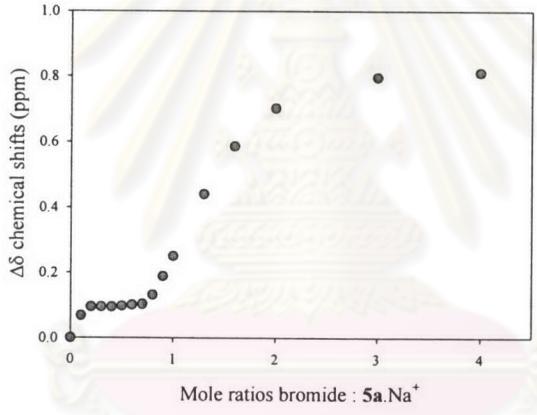

Figure 3.10 The ^{1}H-NMR titration curve of **5a**.Na^+ towards bromide ion on the chemical shifts of a NH proton

We attributed this reduction in host/anion binding to the ion pairing effect. Ion pairing with a competing cation diminished anion basicity and can lower host/anion association constants by two ways.

1. The metal cation can sterically hinder the host/anion interaction. This steric effect increases with the degree of ion pairing.

2. The associated cation lowers the effective charge of anions by either a polarization or shielding effect. This electrostatic effect also increases with the degree of ion pairing.

Finally, we summarized the effect of Na^+ that plays a number of different roles as follows:

1. Organize elements in the receptor. The sodium complexation of ligand **5a** induces a structural change into preorganized structure of urea moieties for binding anions.

2. A co-bound guest in the ion pair receptor that enhances the anion affanity of the receptor (positive allosterric)

3. A competitor with ligand **5a** to form an ion pair with an anion. Na^+ interacts with anions to form an ion pair that diminishes anion basicity and decreases the anion binding ability (negative allosteric).

ศูนย์วิทยทรัพยากร
จุฬาลงกรณ์มหาวิทยาลัย

3.3.4 Complexation studies of ligand 5a in the presence 1.2 equivalents of an anion such as chloride, bromide, iodide, nitrate, acetate, benzoate, and dihydrogen phosphate toward Na^+

In this section, the Na^+ binding properties of ligand **5a** were investigated in order to evaluate the influence of the anion complexations. Addition of Na^+ to the solution of ligand **5a** in the presence of 1.2 equivalents of various anions caused slightly upfield shift of all protons of oxyethylene and methoxy protons in all cases. The stoichiometries and complex formation constants were determined by using the EQNMR program and summarized in Table 3.4. The ^{1}H-NMR titration curves of the titrations are depicted in Figure 3.11

Table 3.4 Na^+ binding of ligand **5a** in the system with presence of 1.2 equivalents of various anions

5a.anion	**K (M^{-1})***
Chloride	283
Bromide	283
Iodide	298
Nitrate	-
Acetate	a
Benzoate	a
Dihydrogenphosphate	a

* Association constants are the average of all ligand **5a,** which exhibited significant complexation induced shifts (uncertainly 10%)

[a] Association constants is too less to be determined.

In all cases, the stoichiometry is 1:1 as confirmed by Job's plots, excepting in the case of presence of NO_3^- exhibited the Na^+/**5a**.NO_3^- of 1.5:1 (as shown in Figure 3.12). That suggested the equilibrium between a 1:1 and a 1:2 complex, and no association constant could be determined.

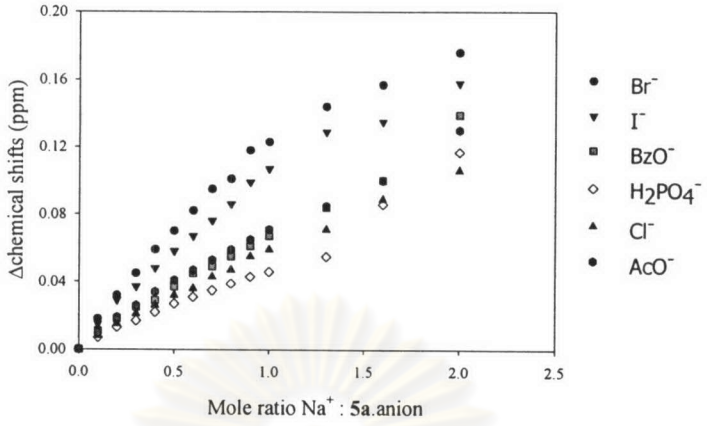

Figure 3.11 The ^{1}H-NMR titration curves of **5a**.anion towards Na^+ on the chemical shifts of an oxyethylene proton

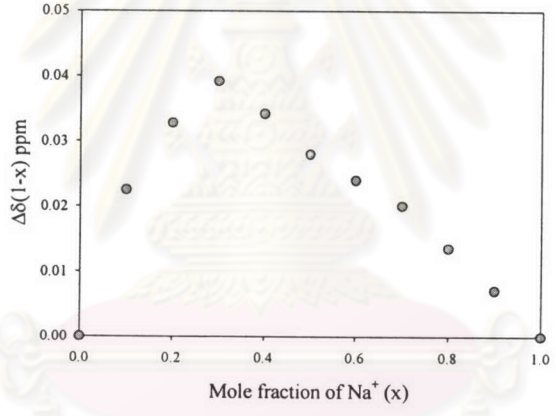

Figure 3.12 Job's plot of the complexation of **5a**.NO_3^- toward Na^+ on the chemical shifts of an ethyleneoxy proton

The sodium complexation affinities of ligand **5a** were decreased from 441 M^{-1} to 283 M^{-1} in the presence of 1.2 equivalents of Cl^- and Br^- and to 298 M^{-1} in the case of I^-. These results suggested that the decrease in Na^+ binding abilities was not governed by size or anion basicity. We attributed these results to the rigid structure of anion complexes and the preorganized poly(oxyethylene) moiety that were not appropriate to bind Na^+. In addition, the poly(oxyethylene) moiety is not flexible enough to organize themselves for binding Na^+ (as shown in Figure 3.13)

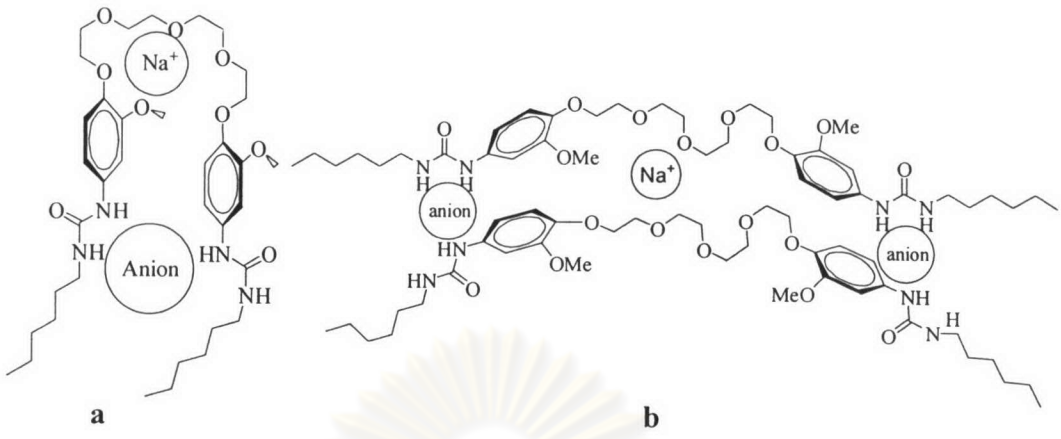

Figure 3.13 The purposed complex structure of ligand **5a**.anion,
a) 1:1 anion complexation, b) 2:2 linear anion complexation with Na^+

On the other hand, comparison with $H_2PO_4^-$, AcO^- and BzO^- bound with ligand **5a** to form stronger complexes than spherical anions. Rigid structures of anion complexes cause the organization of the poly(oxyethylene) moiety unappropriate for binding with Na^+. Thus, dramatic decreases of cation association constants were obtained in the presence of these anions. Hence, the stronger anion complexation increase, the smaller Na^+ binding abilities in this system are obtained. Furthermore, in this case, the anion geometry may participate to alleviate cation binding ability by a steric hindrance caused by the host-anion/Na^+ interaction. This steric effect inhibited the Na^+ binding toward the poly(oxyethylene) moiety, consequently increased the ion pairing between Na^+ and anions.

It can be concluded that the decrease of sodium binding ability of ligand **5a** might be due to the following reasons:

1. Sterically hindered anion geometry that obstructs the entering of Na^+ to approach the cation binding sites cause Na^+ to interact with an anion to form an ion pair.

2. Unsuitable cation binding sites resulted from anion induced organization of the poly(oxyethylene) moiety

3.4 The complexation studies of ligand 5b by using UV-vis titrations

Interactions between ligand **5a** and guests have been generally studied by ^{1}H-NMR titration. However, this method suffers from low sensitivity resulting from the relatively high concentrations in both hosts and guests required in order to obtain NMR signals (10^{-2}-10^{-3} M or more). Moreover, ^{1}H-NMR signals of the active hydrogen (generally NH) measured becomes very broad upon the complexation of anions and overlapping with the aromatic peaks, thereby, making it somewhat more difficult to determine the stability constant of the complex by this method.

Thus, ligand **5b** has been developed to another kind of host that placed *p*-nitrophenyl moieties as an optically UV-vis responsive unit instead. Herein, we report the synthesis (as described in the section 3.2) and binding properties of ligand **5b** by using a UV-vis titration technique.

3.4.1 The structural conformation and the characteristic absorption of ligand 5b in DMSO

Solvent-dependent conformation changes in poly(oxyethylene) linker were investigated by theoretical as well as experimental methods. It is reported that the carbon-carbon bond of the $-OCH_2CH_2O-$ units exists predominantly in the guache conformation in a high polar medium.[49-51]

Ligand **5b** in DMSO probably adopted the conformation as shown in Figure 3.14. Tetraethylene glycol is in a gauche conformation, which results in a higher dipole moment for the poly(oxyethylene) chain and also associates with a more expanded structure for the chain. Futuremore, *p*-nitrophenyl moieties are possible to form a face to face or slightly parallel stacking with phenyl rings of ligand **5b** at the ends of podand by π–π interactions.

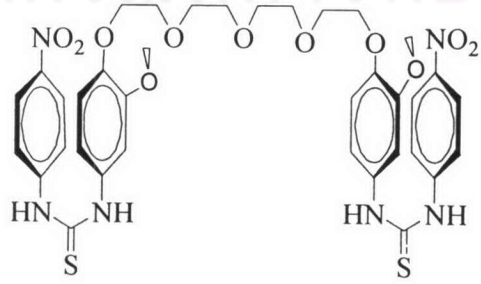

Figure 3.14 The purposed structure of ligand **5b** in DMSO

The characteristic spectra of $2x10^{-5}$ M of ligand **5b** according to a light yellow solution in DMSO shows a broad band around 361 nm (as shown in Figure 3.15). The absorbance of this band follows Beer Lambert law and the molar coefficient of ligand **5b** at 361 nm is 12338 cm^{-1}. This attributes to the π–π^* excitation of *p*-nitrophenol.

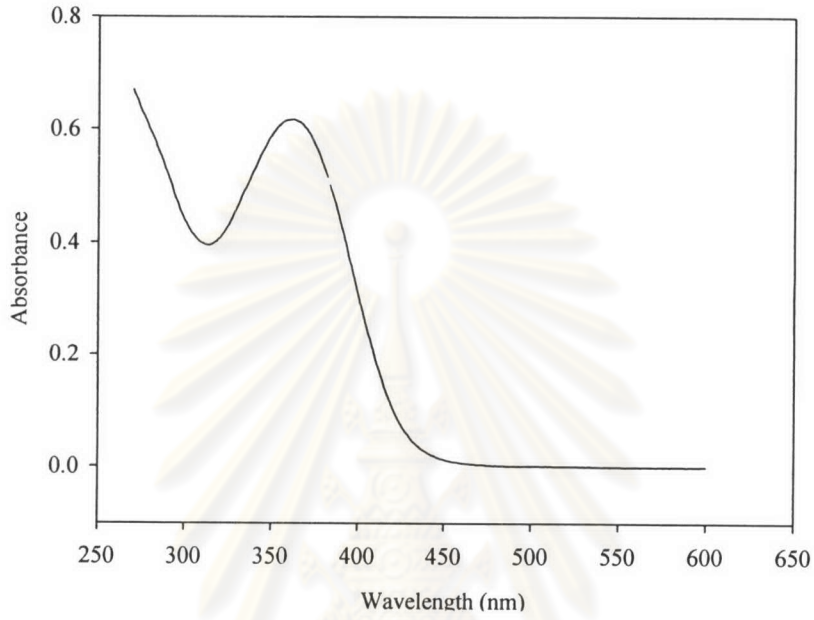

Figure 3.15 The UV-vis absorption spectra of ligand **5b** (2 X 10^{-5} M)

ศูนย์วิทยทรัพยากร
จุฬาลงกรณ์มหาวิทยาลัย

3.4.2 Cation complexation studies.

Absorption spectra of **5b** were measured in DMSO in the absence and presence of an alkali metal ion (sodium and potassium as perchlorate salt and cesium and rubidium as hexafluorophosphate salt) at ambient temperature.

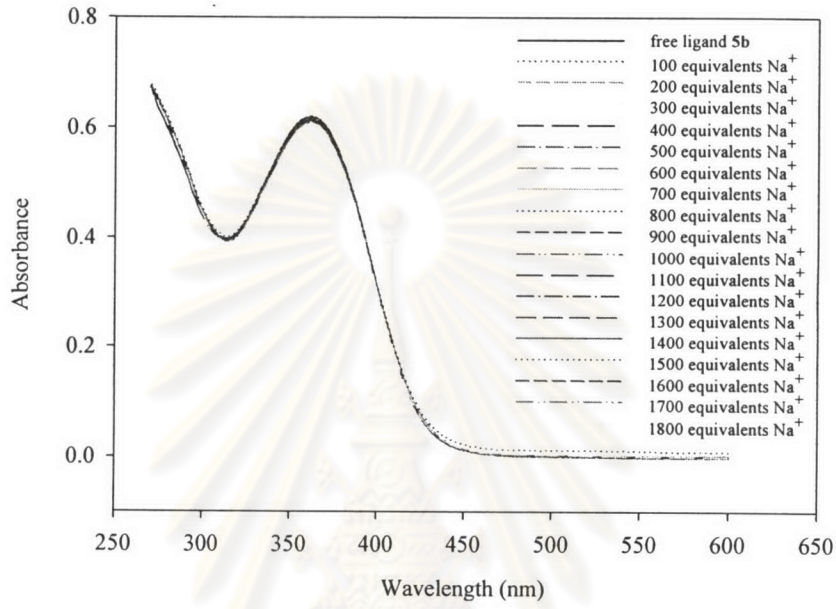

Figure 3.16 Absorption spectra of ligand **5b** upon addition of sodium perchlorate

From titrations between alkali metal ions and ligand **5b**, changes in spectra were not notable even by adding excess amount of an alkali metal ion (for an example as shown in Figure 3.16). This implies that ligand **5b** has not enough affinity for binding alkali metal ions in DMSO. Moreover, the coordination of alkali metal ions gave relatively small electronic perturbation of ligand **5b** that was undetectable by using UV-vis spectroscopy. These results may be due to the influence of the solvation effect with high solvation energy. It is known that cation interacts fairly strong with DMSO via ion-dipole interactions. This also corresponded to any investigations, in which a low binding affinity in a high polar media was found. In addition, the uncomplex form of ligand **5b** in DMSO, the etheric moieties were in gauche conformation (as described above) which exhibited unfavorable degree of host rearrangement. Thus both enthalpic and entropic contributions were unfavorable for the stability of alkali metal complexes of ligand **5b**.

However, we presumed that when ligand **5b** was treated with an alkali metal ion, the structural change of ligand **5b** was converted from the linear polyethylene glycol to pseudocyclic crown ether induced by an alkali metal ion, moreover intramolecular hydrogen bonding between the thiourea moieties possibly occurred as shown in Figure 3.17.

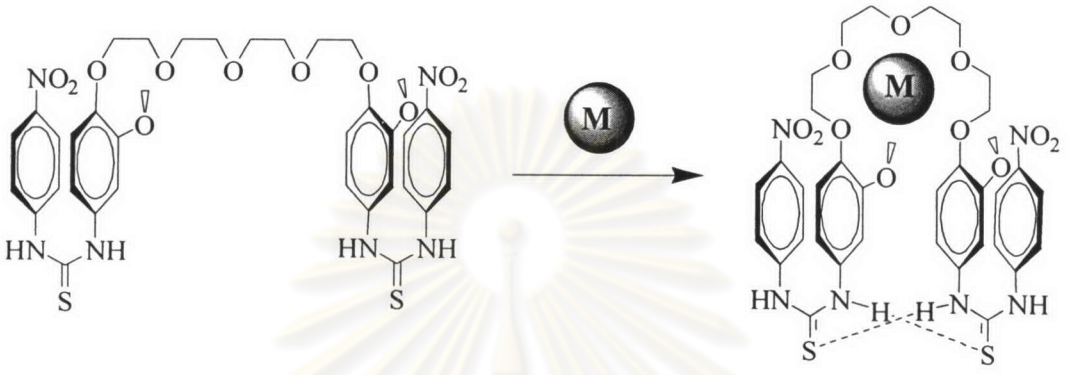

Figure 3.17 The structural change of ligand **5b** induced by an alkali metal ion

ศูนย์วิทยทรัพยากร
จุฬาลงกรณ์มหาวิทยาลัย

3.4.3 Anion complexation studies

The anion complexation abilities of ligand **5b** with various sizes, geometries, and basicity of anions such as chloride, nitrate, benzoate, dihydrogen phosphate, etc. were investigated by using the UV-vis titrations in DMSO.

Otherwise noted, the stoichiometries and binding constants of complexes could be determined from changes in photophysical properties induced by a guest binding. It turned out to be convenient to monitor changes in absorbance at the wavelength corresponding to the maximum absorption of the ligand at 361 nm in DMSO for evaluating of complex formation constants and stoichiometries from the absorption data by using the SIRKO program[52] which were collected in Table 3.5.

Table 3.5 Summary of complex formation constants and stoichiometries (log K) of ligand **5b** for various anionic guests

anionic guest	stoichiometry (host:guest)	log K
Cl^-	1:1	1.93
Br^-	1:1	1.98
I^-	1:2	3.14
NO_3^-	1:1	2.20
BzO^-	1:1, 1:2	$\log K_1 = 4.40$, $\log K_2 = 9.46$
$H_2PO_4^-$	1:2	7.02
ClO_4^-	-	not determined
PF_6^-	-	not determined

In the case of spherical anions such as Cl^-, Br^- and I^-, when addition of the excess amount (1800 equivalents) of an anion as tetrabutylammonium salt displayed a little change in absorbance and no shifts in λ_{max}. For an example, Figure 3.18 presents changes in absorption spectra of ligand **5b** upon addition of Br^-. In the case of **5a**.Cl^-, not only the absorbance at 361 nm decreased but also shifted to 367 nm (as shown in Figure 3.19). However, no color change was observed in these cases.

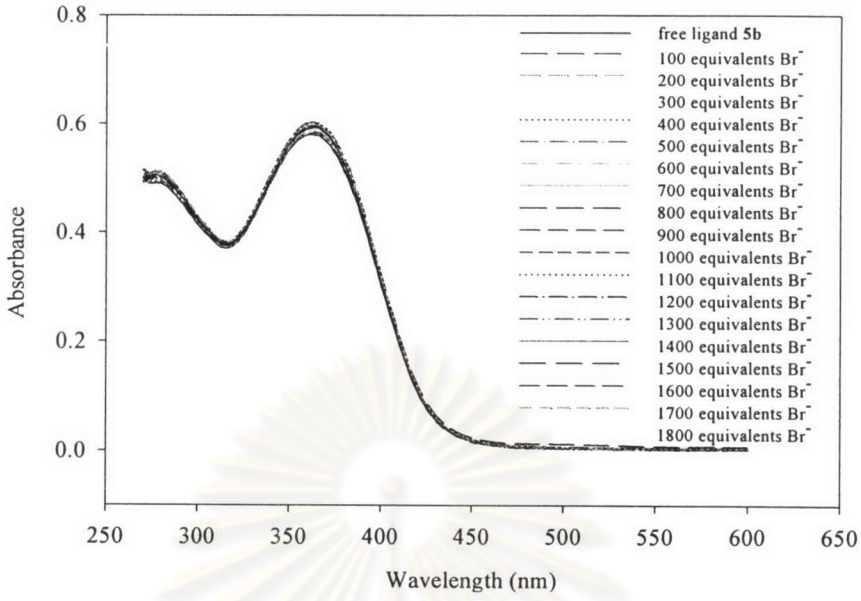

Figure 3.18 Absorption spectra of ligand **5b** upon addition of Br^-

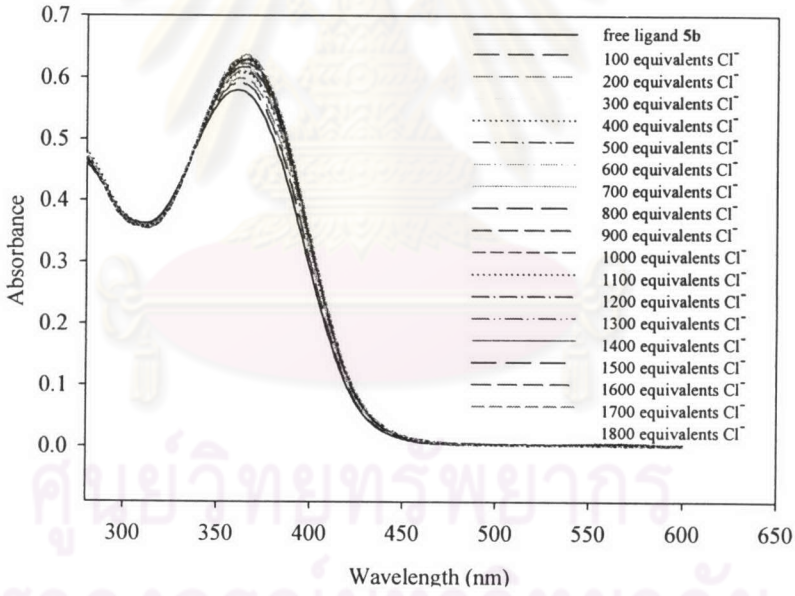

Figure 3.19 Absorption spectra of ligand **5b** upon addition of Cl^-

The UV-vis titrations between ligand **5b** and Cl^- and Br^- were well fitted with an equation assuming in non-linear least square fitting method, that were only induced by the formation of a 1:1 complex host-guest stoichiometry which had binding constants of log K = 1.93 and log K = 1.98, respectively. The possible structure of the complex is shown in Figure 3.20.

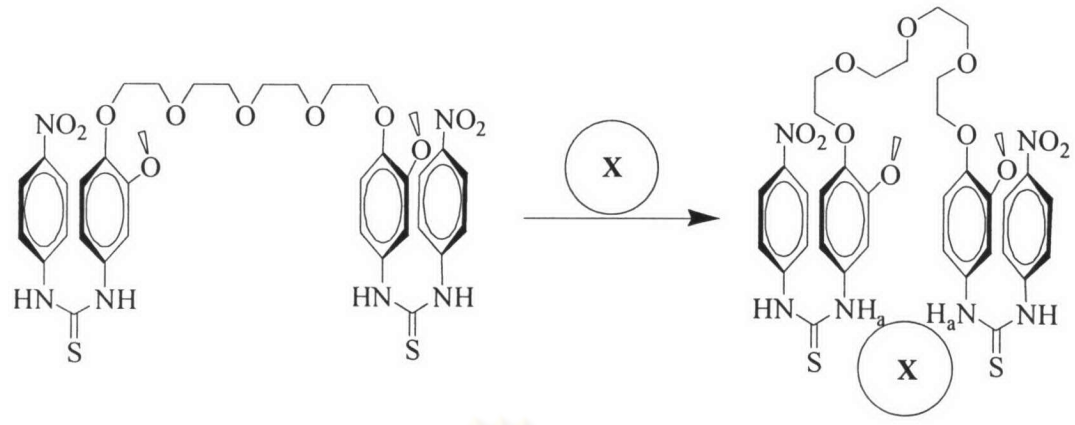

Figure 3.20 The purposed 1:1 complex structure of **5b**.X where X = Cl^- or Br^-

Unlike Cl^- and Br^-, I^- could not associate into the cavity between NH_a groups of thiourea but bind mainly on each thiourea group as shown in Figure 3.21. The stoichiometry of **5b**.I^- was thus in a 1:2 ratio with the association constant of log K = 3.14.

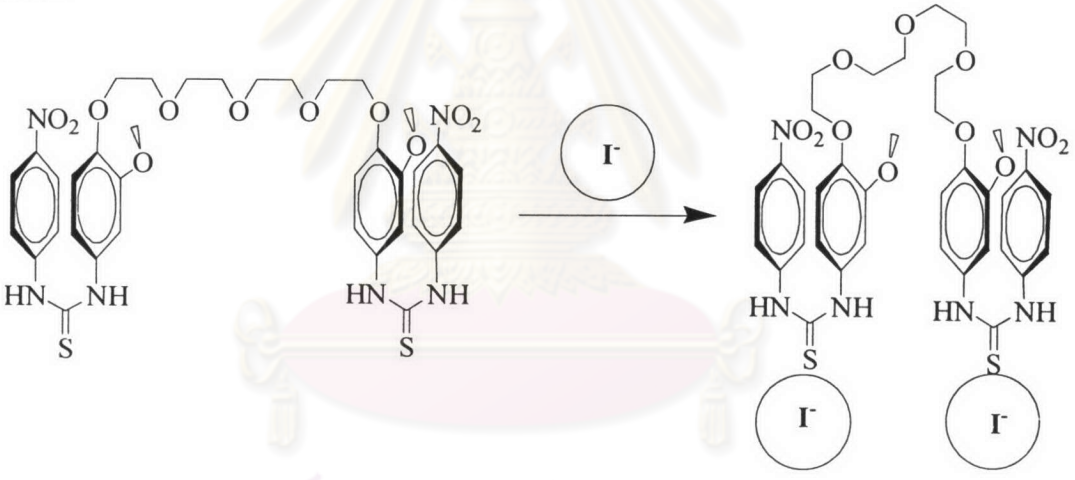

Figure 3.21 The purposed 1:1 complex structure of **5b**.I^-

Addition of NO_3^- with the equal amount of above anions showed no remarkable changes in the color and the absorbance at 361 nm but significantly changing of absorbance around 316 nm occurred due to the absorption of tetrabutylammonium nitrate anion (as shown in Figure 3.22). The stoichiometry of the **5b**.NO_3^- was found to be 1:1 with the stability constant of log K = 2.2. The structure was proposed to be like **5a**.Cl^- or **5a**.Br^- which two oxygen atoms of NO_3^- bound with NH_a group of each thiourea (as shown in Figure 3.23).

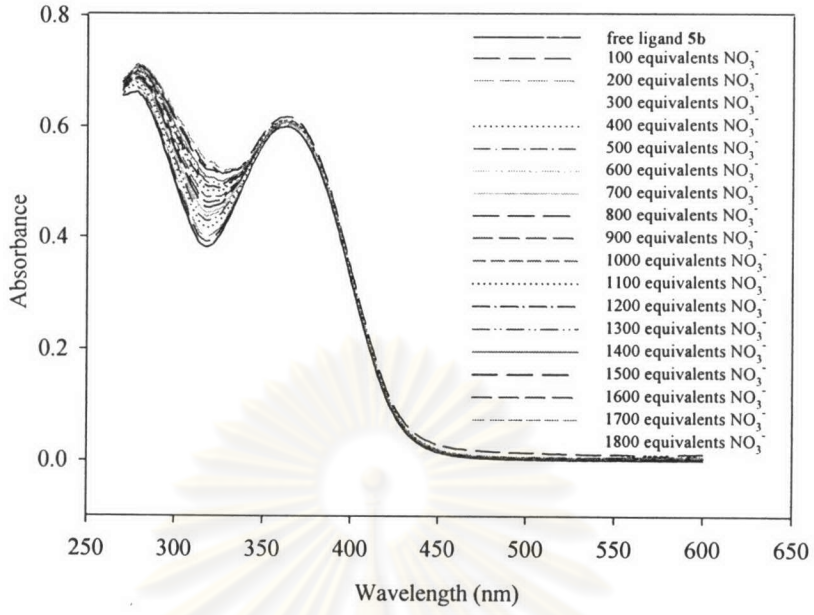

Figure 3.22 Absorption spectra of ligand **5b** upon addition of NO_3^-

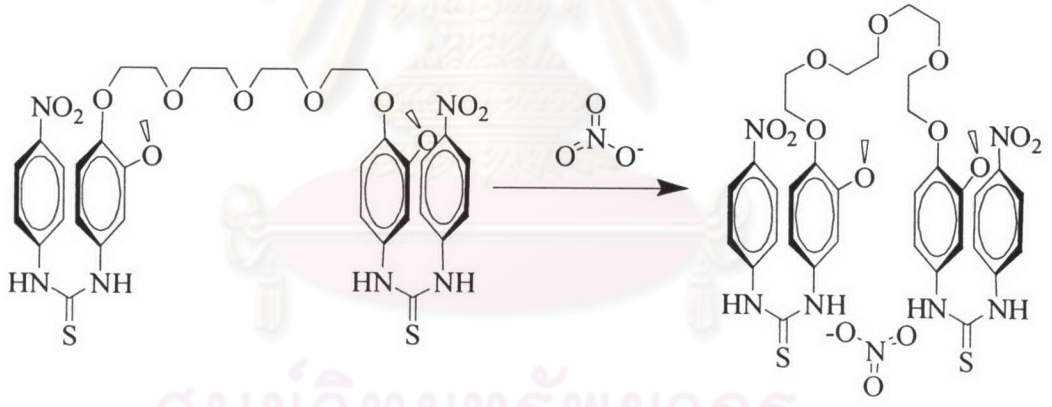

Figure 3.23 The purposed 1:1 complex structure of **5b**.NO_3^-

On the other hand, upon addition of BzO^- (trigonal planar geometry as NO_3^-) the band at 361 nm decreased and moved to longer wavelength reaching maximum value at 459 nm by addition 6 equivalents of BzO^-. Unclear isobestic point (Figure 3.23) was observed with concommitant of the color of the solution changed from light yellow to deep red-orange. The phenomena suggested that the complexation occurred and more than one species formed, corresponding to the best fit with the complexation models 1:1 and 1:2 (host: guest) and log K_1 = 4.40 and log K_2 = 9.46, respectively.

However, the species distribution in Figure 3.25 exhibit the predominance species of 1:2 complex with 50% conversion and the minor 1:1 formation around 20% conversion.

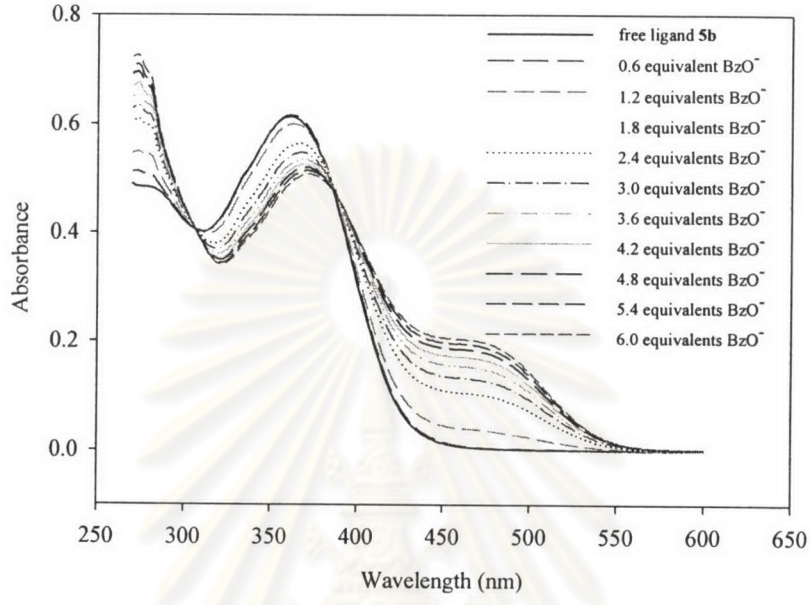

Figure 3.24 Absorption spectra of ligand **5b** upon addition of BzO^-

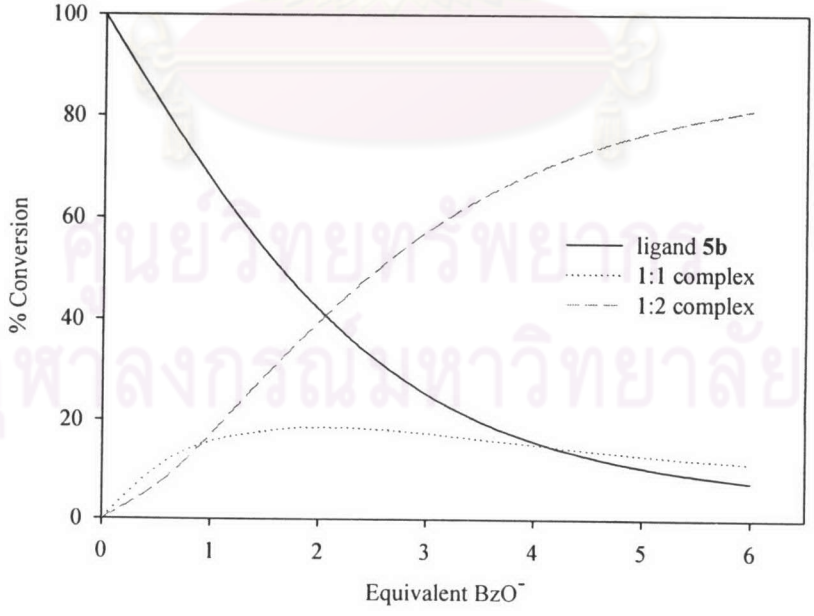

Figure 3.25 Species distribution of **5b**.BzO^- complexes

Although BzO^- and NO_3^- possessed in similar anion geometry, but the stoichiometry was obtained in a different fashion. This can be explained based on the different structure of anions. BzO^- is an aromatic anion that binds ligand **5b** stronger than NO_3^- because π–π interactions between phenyl rings of BzO^- and phenyl rings of ligand **5b** enhances the anion binding abilities. Possible structures of 1:1 and 1:2 complexes are shown in Figure 3.26.

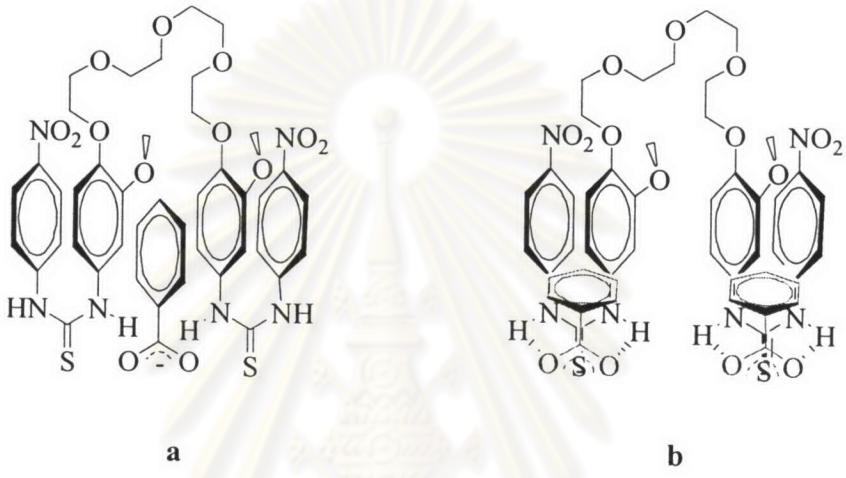

Figure 3.26 The purposed a) 1:1 complex and b) 1:2 complex structure of **5b**.BzO^-

The titration of ligand **5b** with $H_2PO_4^-$ lead to a drastically change in color and absorption as the same as observed in the case of BzO^- (Figure 3.27). These absorbance data gave only a 1:2 stoichiometry (host: guest) with stability constant of log K = 7.02. Consequently, the binding model of a 1:2 complex was preferred more favorable than the insignificant species of 1:1 complex that may occur rapidly and too fast to be detected. We propose the complexation structure of the complex as shown in Figure 3.28.

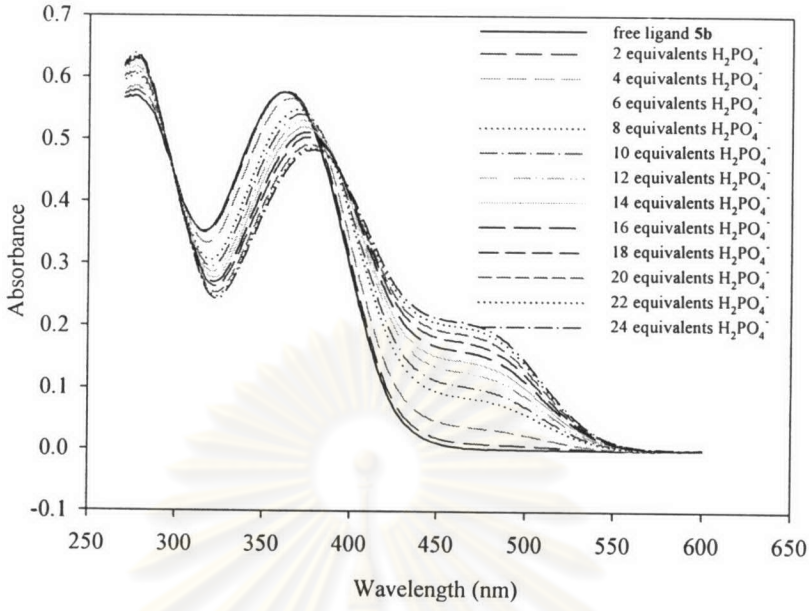

Figure 3.27 Absorption spectra of ligand **5b** upon addition of $H_2PO_4^-$

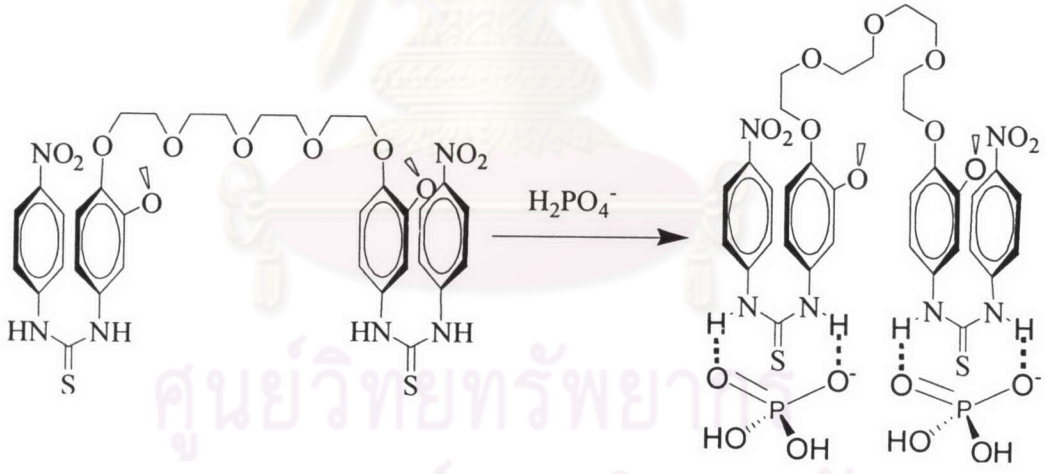

Figure 3.28 The purposed 1:2 complex structure of **5b**.$H_2PO_4^-$

Unfortunately, in the case of AcO^-, we could not fit the titration curve by SIRKO program. However, addition of AcO^- induced the color change as in the cases of BzO^- and $H_2PO_4^-$. In fact, the plot between the absorbance versus the equivalents of anion was similar to an acid-base titration curve. It is possible that there might be pH changes during the titration which was actually found in the previous work of our group.[54] The abrupt change in absorbance observed at 38 equivalents thus could be

resulting from the deprotonation of the ligand, considering the fact that AcO^- are basic and that ligand **5b** contains deprotonable groups. On the other hand, It is possibly due to the input of binding models into this program that were not improper for fitting the experimental results as a consequence of complicate systems in which more than one species and phenomena could occurred such as 1:1, 1:2 complexes, anion coordination and acid-base interaction. Furthermore, the larger anions such as ClO_4^- (tetrahedron geometry) and PF_6^- (octahedron geometry) were investigated. The results showed no remarkable shifts in absorption spectra and no variation of absorbance, indicating no sign of complexation with these anions. In addition, the anionic radii were larger than the cavity of ligand **5b**. Interestingly, the color change is remarkable in 1:2 complexes. This is due to anion associated directly on each thiourea moiety which influentially perturbed electronic properties of the nitrophenol moieties.

We conclude the order of the formation constants of **5b** with anions were NO_3^- > Br^-~ Cl^- for 1:1 complexes and BzO^- > $H_2PO_4^-$ >> I^- for1:2 complexes. These trends agree with in the results of our previous work with ligand **5a** by using NMR titration method (as describe in section 3.3.2). That suggested the anion binding abilities of ligand **5b** also depended on anion geometry as well as hydrogen bonding sites of anions.

It is should be noted that ligand **5b** exhibited the selectivity of anion-induced dramatic color change to BzO^- and $H_2PO_4^-$ over other anions. It is thus possible able to use ligand **5b** as a naked eye sensor. However, ligand **5b** cannot discriminate the degree of color change between BzO^-, AcO^- and $H_2PO_4^-$.

ศูนย์วิทยทรัพยากร
จุฬาลงกรณ์มหาวิทยาลัย

3.4.4 Complexation studies of ligand 5b in the presence of 500 equivalents of an alkali metal ion ($NaClO_4$ and $KClO_4$) toward various anions.

UV-vis titration experiments were carried out repeatedly in the presence of 500 equivalents of an alkali metal ion ($NaClO_4$ and $KClO_4$) for investigating the effects of cations toward the association constant of the various anions. It was found that no significant change in absorption spectrum and color were observed when solution of ligand **5b** in DMSO was exposed to 500 equivalents of an alkali metal ion (Figure 3.29). The stoichiometries and anion complex formation constants were evaluated by using computer program SIRKO and listed in Table 3.6.

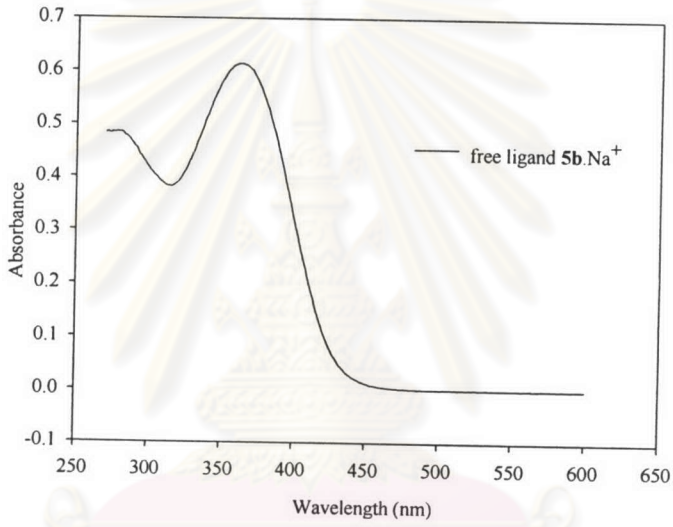

Figure 3.29 Absorption spectra of ligand **5b** upon addition of 500 equiv. of Na^+

Table 3.6 Summary of complex formation constants and stoichiometries (log K) of ligand **5b**.alkali metal ion for various anionic guests

guest	stoichiometry (host:guest)		log K	
	Na^+	K^+	Na^+	K^+
Cl^-	1:1	1:1	1.60	1.80
Br^-	1:1	1:1	1.79	1.89
I^-	1:2	1:1, 1:2	2.73	$\log K_1 = 1.72$, $\log K_2 = 3.58$
NO_3^-	1:1	1:1	2.91	2.31
BzO^-	1:2	1:1, 1:2	8.75	$\log K_1 = 5.58$, $\log K_2 = 9.17$
$H_2PO_4^-$	1:2	-	6.37	not determined

In the case of spherical ions such as Cl^-, Br^- and I^-, aliquots of an anion as tetrabutylammonium salt were added to a solution of ligand **5b** in the presence of 500 equivalents of an alkali metal ion ($NaClO_4$ or $KClO_4$) with the equal amount of anions in section 3.4.3. Resulted spectra changes were the same as the system of absence an alkali metal ion and no color change was observed. For an example, Figure 3.30 displays changes in the absorption spectra of **5b**.Na^+ upon addition of Br^-. In each case, the stoichiometries were obtained by fitting the titration isotherm to 1:1 binding model for Cl^-, Br^- and both 1:1 and 1:2 for I^- and the association constants are collected in Table 3.6.

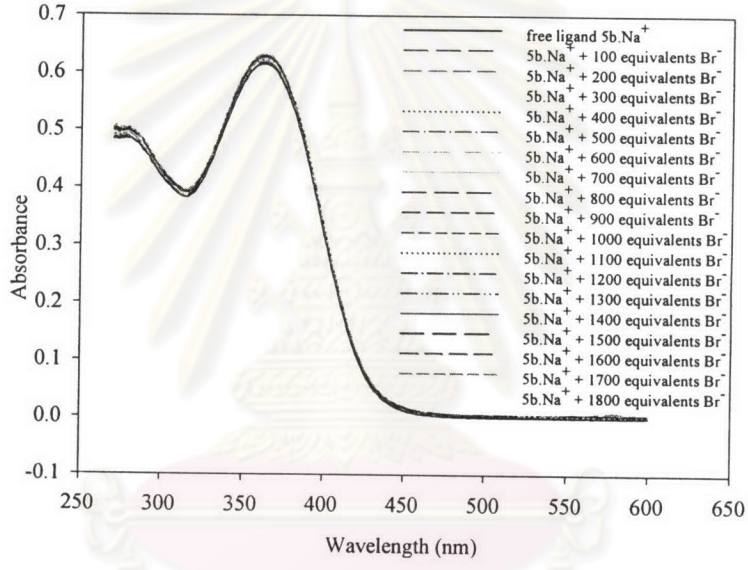

Figure 3.30 Absorption spectra of ligand **5b**.Na^+ upon addition of Br^-

In all cases, calculated anion affinity constants were substantially decreased by the presence of 500 equivalents of sodium perchlorate than potassium perchlorate, except **5b**.K^+/I^-.

We presumed that when ligand **5b** was treated with an alkali metal ion, the complexation of an alkali metal ion with the podand converted the linear polyethylene glycol chain to pseudocyclic crown ether. Consequently, intramolecular hydrogen bonding between the thiourea moieties possibly occurred and decreased the anion binding abilities of ligand **5b** as shown in Figure 3.17.

Actually, the glyme-5 moiety of ligand **5b** binds Na^+ more stable than K^+ insisted by the fact of the result of our previous work with ligand **5a** by using NMR

titration method described in section 3.3.1. This implies that the intramolecular hydrogen bonding between the thiourea moieties of **5b**.Na^+ complex is stronger than that of **5b**.K^+.

Furthermore, the decrease of anion binding ability was also found in the presence of both alkali metal ions. This indicated that partial alkali metal ion may form ion pairing outside the cavity which competed with ion binding to the receptor.[55] Association constants of **5b**.Na^+/anion decrease more than those of **5b**.K^+/anion. These were ascribed by the ion-pairing ability. For an example of the association constant of **5b**/Cl^-, Na^+ is harder ion preferring to form ion-pair with hard Cl^- than K^+. Thus the determined **5b**.Na^+/Cl^- association constant was less than **5b**.K^+/Cl^-.

However, **5b**.Na^+ complex did not enhance I^- recognition but the **5b**.K^+ complex favored the binding of I^-. These results may pointed out to the large radii of K^+ that **5b**.K^+ complex can enlarge the anion cavity site between NH_a groups of thiourea more than **5b**.Na^+. Subsequently, the intramolecular hydrogen bonding of **5b**.K^+ was weaker compare to **5b**.Na^+ complex. The explanation agrees with the stoichiometry of **5b**.K^+/I^- that was found to be 1:1 and 1:2 complexes. The 1:1 stoichiometry was suggested that the anion cavity at the site between the NH_a groups of thiourea be expanded enough to bind I^- (Figure 3.31).

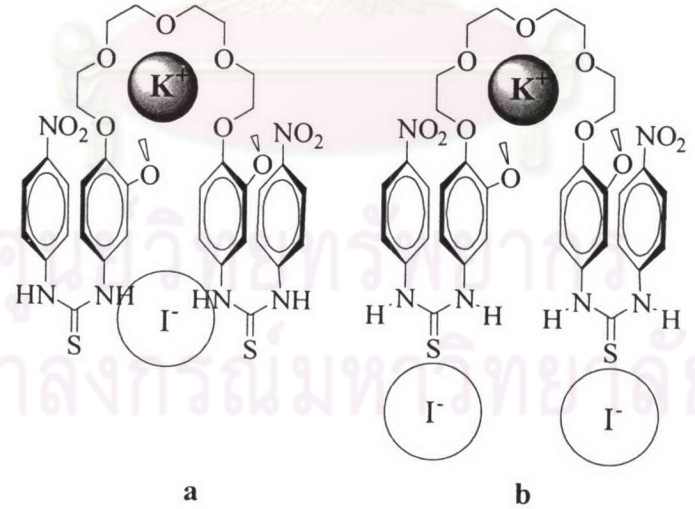

Figure 3.31 The purposed 1:1 complex (**a**) and 1:2 complex (**b**) structure of **5b**.K^+/I^-

However, I^- may not be appropriate to bind **5a**.Na^+ in a 1:1 formation (20% conversion) due to the large radii of I^- (220 pm) but favor to bind in a 1:2 complex (55% conversion) as regarding to the species distribution shown in Figure 3.32. In

contrast to **5b**.Na^+/I^-, we found only 1:2 complex because of the inhibition of a 1:1 anion binding ability by the strong intramolecular hydrogen bonding of the thiourea moieties and the small cavity of the 1:1 anion binding site due to the complexation of **5b**.Na^+.

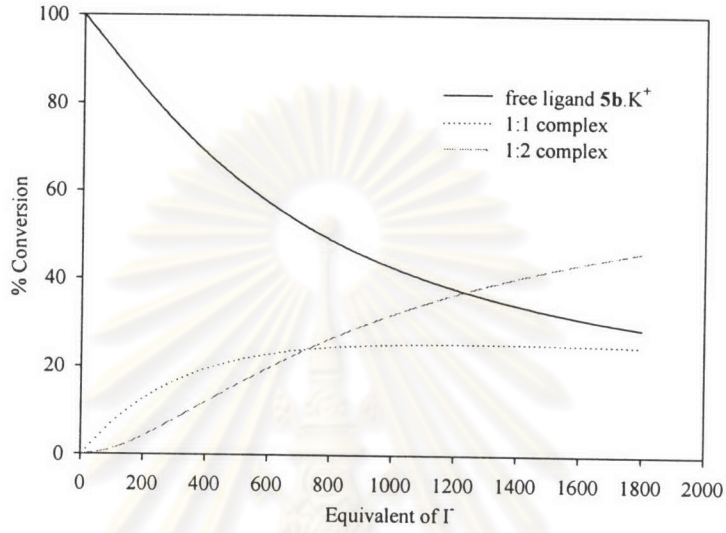

Figure 3.32 Species distribution of **5b**.K^+/I^- complexes

Addition of NO_3^- to a solution of ligand **5b** in the presence of 500 equivalents of an alkali metal ion (Na^+ and K^+) displayed the change in the UV-vis absorption spectra as similar in the absence of an alkali metal ion and no detectable color change is observed upon addition of excess NO_3^-. The best fitting curve gave stability constants for **5b**.Na^+/NO_3^- and **5b**.K^+/NO_3^- as shown in Table 3.6. Interestingly, the anion ability of ligand **5b** in this system in the presence of 500 equivalents of alkali metal ions were slightly increased from log K = 2.2 to 2.91 in the case of Na^+ and to 2.87 in the case of K^+ by fitting the titration isotherm to a 1:1 binding model. The result showed a substantial increase in the NO_3^- binding ability as compared to the free ligand **5b**. This may be due to the suitable arrangement and orientation of oxoanion guests to bind ligand **5b.**

Na^+ or K^+ induced positive cooperatively of NO_3^- binding which can be explained as a consequence of favorable electrostatic attraction between the poly(oxyethylene) moiety bound alkali metal ion and thiourea complexed anion. The possible structure was that 2 oxygen atoms of NO_3^- binded with NH_a group of each thiourea and the rest was probably stabilized by the bounded alkali metal ion via

electrostatic interactions as shown in Figure 3.33., while the other anions have no available coordination site to cooperate the bounded alkali metal ion. The proposed structure of the complex can be explained whereas the stability constants of these complexes were increased and the others decreased. As a matter of fact, the **5b**.Na^+/NO_3^- complex is more stable than the **5b**. K^+/NO_3^- complex because of the hard oxygen prefer to interact with hard Na^+ rather than K^+.

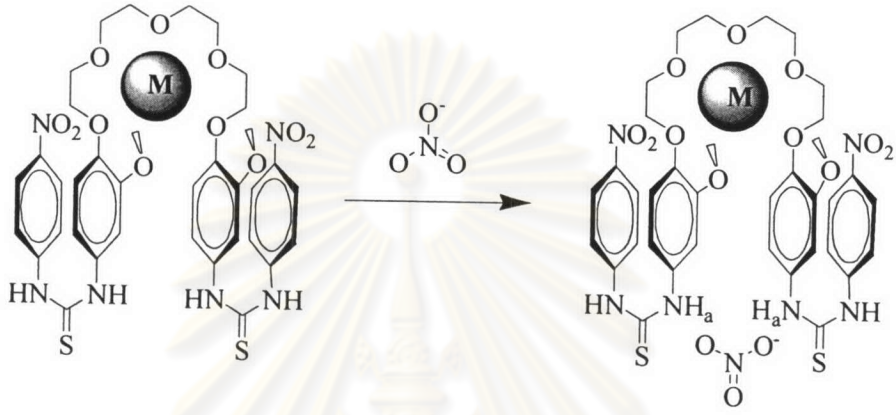

Figure 3.33 The purposed 1:1 complex structure of **5b**.Na^+/NO_3^-

On the other hand, solution of **5b** was titrated with BzO^-. Increasing in BzO^- concentration resulted in a drastically increase of absorbance at around 459 nm and appreciable decrease the absorbance at 361 nm (as similar in the system of absence of an alkali metal ion). Thus the color of solution changes from light yellow to deep red-orange. For an example, the absorption spectra of **5b**.Na^+/BzO^- are shown in Figure 3.34.

The absorbance data of **5b**.Na^+/BzO^- complex was interpreted to obtain only 1:2 stoichiometry with log K = 8.75. In contrast to **5b**.K^+/BzO^- complex, the best fitting curve gave both 1:1 and 1:2 binding models and association constants log K_1 = 5.58 and log K_2 = 9.17. These stoichiometric results can be explained by the same explanation as in the case of I^-.

In the case of **5b**.K^+/BzO^- complex possessed log K_1 higher than the free ligand **5b** and the similar trend in log K_2. Otherwise, the predominance 1:1 species complex with 80% conversion was more favorable than the 1:2 formation with 35% conversion distinguished from **5b**/BzO^- (Figure 3.35). **5b**.K^+ probably induced the suitable cavity size between the NH_a of thiourea groups which phenyl rings were close enough for binding BzO^-. These enhanced the π-π interactions between aromatic

rings of ligand **5b** and aromatic ring of BzO^-. The purposed structure of 1:1 **5b**.K^+/BzO^- complex is shown in Figure 3.36.

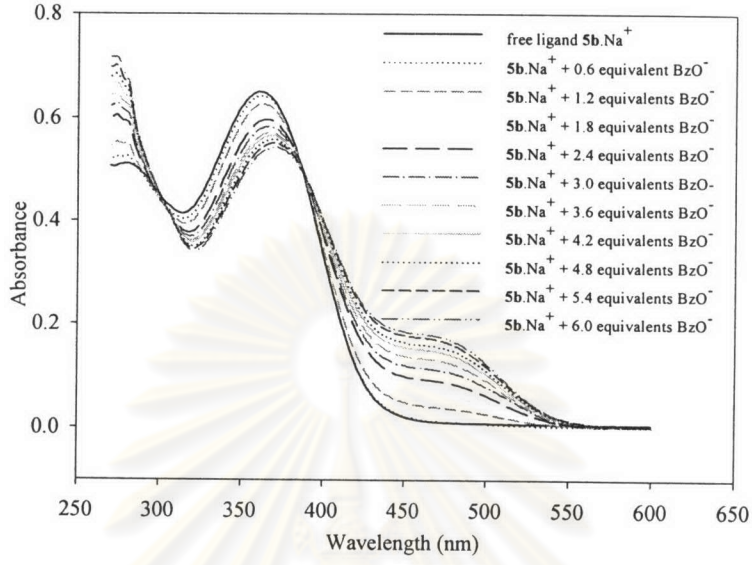

Figure 3.34 Absorption spectra of ligand **5b**.Na^+ upon addition of BzO^-

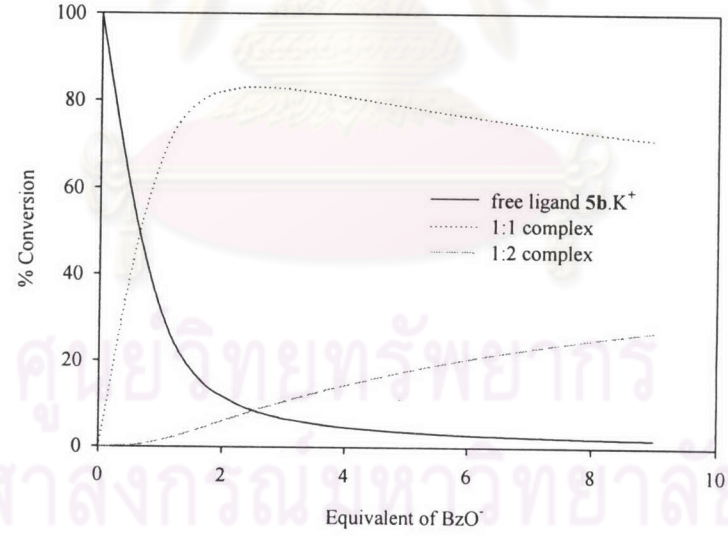

Figure 3.35 Species distribution of **5b**.K^+/BzO^- complexes

It should be noted that **5b**.K^+/BzO^- possessed the association constants higher than that of **5b**.Na^+/BzO^-. The observation can be explained by the ion-pair effect that the ion pair association constant in DMSO of potassium benzoate (48 M^{-1}) is lower than that of sodium benzoate (200 M^{-1}).[56]

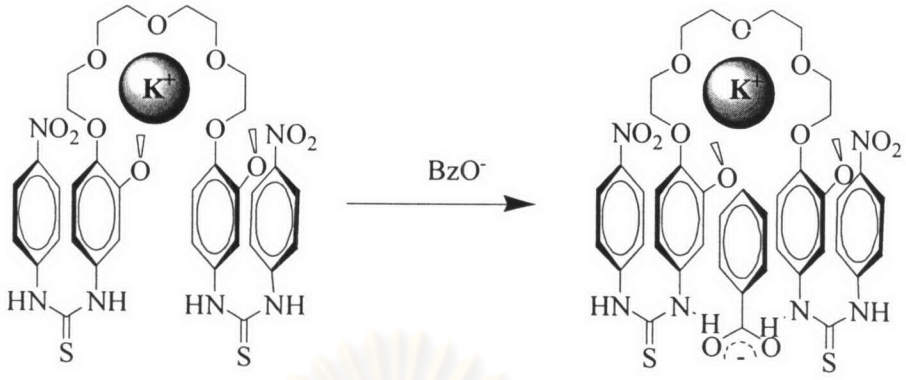

Figure 3.36 The purposed 1:1 complex structure of **5b**.K^+/BzO^-

$H_2PO_4^-$ was also employed to determine the stoichiometries and stability constants in the presence of an alkali metal ion. The results are shown in Table 3.6. Addition of $H_2PO_4^-$ lead to decreasing of the band around 361 nm and unremarkable increasing absorbance at around 459 nm, as shown in Figure 3.37.

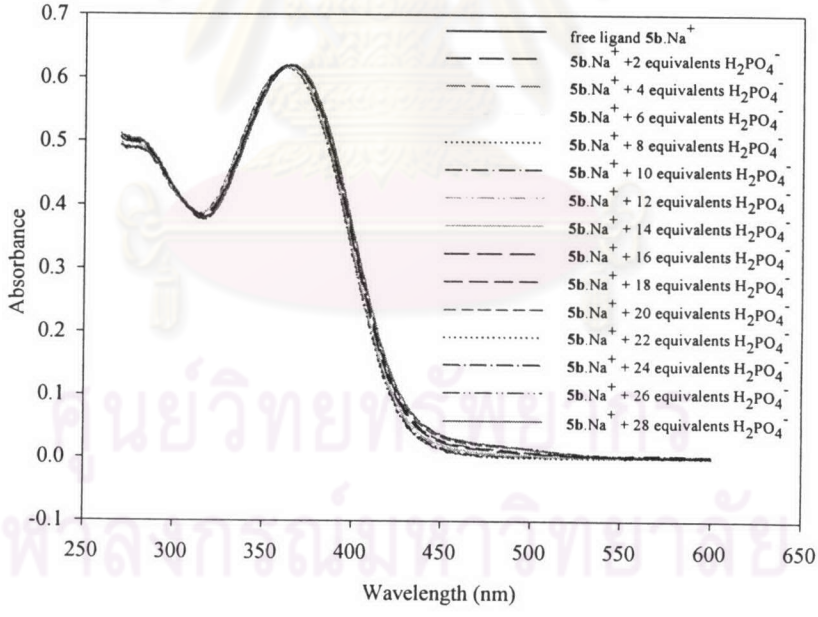

Figure 3.37 Absorption spectra of ligand **5b**.Na^+ upon addition of $H_2PO_4^-$

However, the peak around 459 nm changes insignificantly compared to the system in the absence of an alkali metal ion and the degree of color change was less affected, which turned light yellow to orange. Apparently, these results suggested that

the alkali metal ion behaved as a co-bound $H_2PO_4^-$ to form aggregated ion pair. This diminished anion basicity and reduced the anion binding ability. According to these facts, the complex formation constant for **5b**.$Na^+/H_2PO_4^-$ was indeed reduced approximately by a factor of 10 and cannot be estimated for **5b**.$K^+/H_2PO_4^-$. It is possibly due to the input binding models into this program that were not appreciate for fitting the experimental results as a consequence of complicate system.

The presence of Na^+ substantially reduced the affinity of ligand **5b**/anion over K^+, which can be explained below by a cooperativity factor. The data in Table 3.6 were used to generate a cooperativity factor (Figure 3.38). A cooperativity factor is simply the anion association constant in the presence of an alkali metal ion divided by the anion association constant in the absence of an alkali metal ion.[36] A value < 1 indicates that ligand **5b**/anion binding is inhibited by the ion-pairing and intramolecular hydrogen bonding effect, whereas a cooperativity factor > 1 reflects ligand **5b**/anion binding enhancement due to the ion-pair recognition.

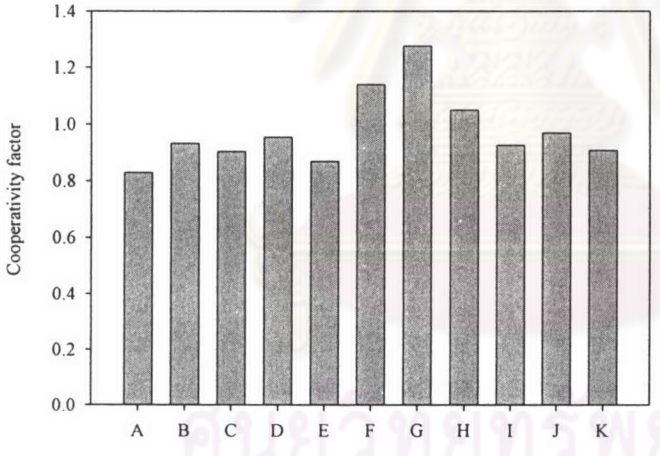

Figure 3.38 Cooperativity factor for ditopic receptor **5b**

Examination of Figure 3.38 reveals two ligand **5b**-independent trends. First, the cooperativity factor for a specific ligand **5b**/anion system increases with decreasing metal cation charge to surface area ratio, i.e. $Na^+ < K^+$. Second, the cooperativity factor for a specific ligand **5b**/anion system increases with decreasing anion basicity, i.e. $Cl^- < Br^- < I^-$ and $BzO^- < NO_3^-$. These trends were in agreement with other studies in analogous heteroditopic receptors containing crown ethers and urea/thiourea groups.[36] Ligand **5b**/anion affinity is reduced by the ion-pairing effect.

In certain cases, when one or both of ions are small and charged localized, this inhibition effect is observed, which suggests that the crown encapsulated cation is able to sequester the anion away from the NH residues of ligand **5b**. However, the stoichiometry of the complex will also affect the observed cooperativity factor, but in these cases, ion pairing plays a crucial role.

Finally, we conclude the anion binding ability of the ligand **5b** in the presence of an alkali metal ion may either enhanced or suppressed depending upon the both natures of the **5b**.alkali metal ion complex and anions including the ion pairing ability between cations and anions.

ศูนย์วิทยทรัพยากร
จุฬาลงกรณ์มหาวิทยาลัย

3.4.5 Complexation studies of ligand 5b in the presence of an anion such as chloride, bromide, iodide, nitrate, benzoate and dihydrogenphosphate toward Na^+ and K^+

In this section, the alkali metal ion binding abilities of ligand **5b** were investigated in order to evaluate the influence of the anion complexation by repeating the titration in the presence of an anion. It is remarkable that the characterization spectrum of ligand **5b** in the presence of 2000 equivalents of a spherical anion such as Cl^-, Br^- and I^- showed an absorption maximum at 361 nm like the spectrum of free ligand **5b**. Typically, solutions of **5b**.anion were titrated with an alkali metal ion resulting in no remarkable change similar to the system without of anion. For an example, Figure 3.39 illustrates changes in absorption spectra of ligand **5b**.Br^- upon addition of Na^+. This implied that alkali metal ions could not bind well with ligand **5b** in the presence of above mentioned anionic species and stability constants of the complexes of ligand **5b**.anion/alkali metal ion could not be determined by analysis of the absorption spectra. The complexation of ligand **5b** with alkali metal ions in the presence of these anions was probably inhibited by the ion pairing effect.

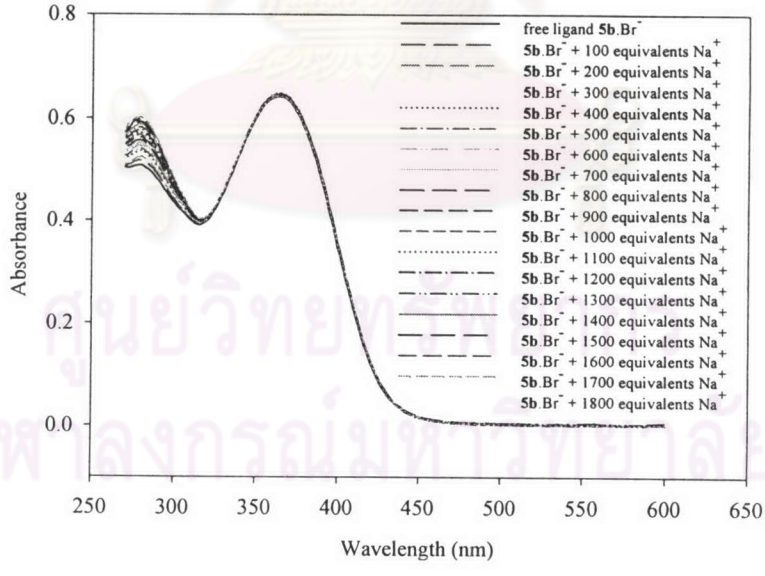

Figure 3.39 Absorption spectra of ligand **5b**.Br^- upon addition of Na^+

The structure of ligand **5b** is dominantly in the unorganized poly(oxyethylene) moiety and causes the less appropriate pseudocyclic ring for binding alkali metal ions. Upon addition of an alkali metal ion, anions probably dissociated from coordinated thiourea inducing by added alkali metal ion and formed ion pairing that prevented alkali metal ions to coordinate the oxyethylene glycol chain.

Furthermore, alkali metal ions cannot induce complementary organization of the poly(oxyethylene) moiety to complexation. This is probably due to the rigid structure of anion complexes. Therefore, the alkali metal ion preferred to bind an anion more strongly than to bind the poly(oxyethylene) moiety, resulting in ion-pairing.

In the case of $H_2PO_4^-$, the spectra are reversible upon addition of an alkali metal ion that reflected the reversibility of anion sensing. The added alkali metal ion dissociated $H_2PO_4^-$ from the coordination of thiourea. This produced a blue shift of absorption spectra of **5b**.$H_2PO_4^-$ complex and reverted to the original spectrum as free ligand **5b**. When an alkali metal ion was added to a solution of ligand **5b** containing $H_2PO_4^-$, the absorbance of the broad absorption maximum at 459 nm decreased with concommitant growth of the reversible blue shifted band at 361 nm (Figure 3.40), that almost exactly coincide with the spectrum of the free ligand **5b** and the color returned from deep red-orange to yellow. These changing processes reverse the processes described in section 3.4.4 (addition of $H_2PO_4^-$ to the solution of ligand **5b** containing an alkali metal ion).

It should be noted that the differences of these responses in the sequence of guest addition were employed in their applications described in section 3.5. The changes in spectra confirm that ion-pairing occurred in this system. The anion basicity was reduced by ion-pairing that strongly decreased the anion coordination properties of ligand **5b**, causing the spectra change reversion to the original spectrum of free ligand **5b**.

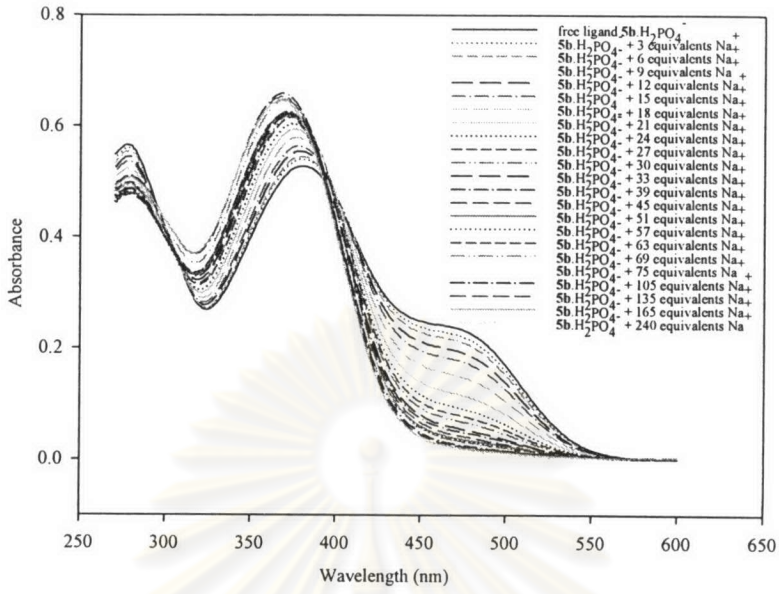

Figure 3.40 Absorption spectra of ligand **5b**.$H_2PO_4^-$ upon addition of Na^+

Solutions of **5b**.NO_3^- were titrated with an alkali metal ion. The increase in alkali metal ion concentration resulted in a decreasing of absorbance of tetrabutylammonium nitrate around 316 nm. These phenomena reflected that an alkali metal ion probably associated to NO_3^-. Interestingly, the alkali binding abilities of ligand **5b** in the system in the presence of 2000 equivalents of NO_3^- were increased to 2.91 in the case of Na^+ and to 2.87 in the case of K^+ by fitting the titration isotherm to a 1:1 binding model. Apparently, the increasing of the association constants were to be anticipated from an oxygen atom of nitrate ion which probably stabilized via electrostatic interactions of the bounded alkali metal ion. The association of Na^+ in this system exhibited a slightly greater value than that of K^+ that corresponding to the purposed structure of the complex as a consequence of the hard Na^+ prefer to interact with hard oxygen atoms of NO_3^- over than K^+.

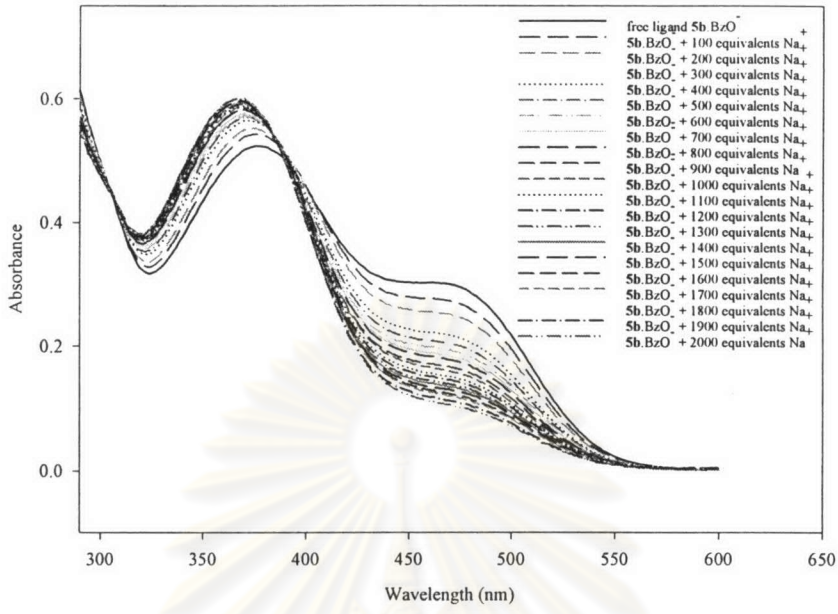

Figure 3.41 Absorption spectra of ligand **5b**.BzO^- upon addition of Na^+

In the case of **5b**.BzO^-, it was found that addition of Na^+ and K^+ increased the binding constants to log K = 2.40 and log K = 2.25, respectively. In this case, we also found reversible spectra upon addition of alkali metal ions that produced a blue shift of the absorption spectra similar to that observed in the $H_2PO_4^-$ case. Nevertheless, the decreasing absorbance of the broad absorption band at 459 nm was not completely reversible as in the case of $H_2PO_4^-$ and did not congruently coincide with the spectrum of the free ligand **5b** (Figure 3.41) . That was due to BzO^- bound tightly with ligand **5b** to form a strong complex than other anions. Therefore, ion pairing between alkali metal ions and BzO^- was inhibited.

On the other hand, when compared the alkali binding ability of ligand **5b** in the presence of NO_3^- and BzO^-, the former system displays higher enhancement than the latter system. This can be possibly rationalized by directly favorable electrostatic interactions of oxygen of NO_3^- which urged the cation to coordinate to the poly(oxyethylene) moiety of ligand **5b**.

Finally, we summarized the influence of the anion complexation toward alkali binding ability of ligand **5b** as follows:

1. Decreasing in cation association constants occurred with the weak anion complexes. Consequently, anions were probably withdrawn from thiourea coordination and formed ion pairing inducing by the added alkali metal ions. Furthermore, the unorganization of poly(oxyethylene) moiety and rigid structure of anion complexes may cause the increase in ion pairing, which decreased alkali binding ability of ligand **5b**.

2. Increasing in cation association constants, these phenomena may occurred with the strong and appropriate anion complexes, which could diminished the ion pairing effect and induced alkali metal ions to coordinate with the poly(oxyethylene) moiety by a secondary interaction such as electrostatic interactions.

ศูนย์วิทยทรัพยากร
จุฬาลงกรณ์มหาวิทยาลัย

3.5 The application of ligand 5b

Photodriven supramolecular systems are useful for information gathering (sensing), storage, processing, and transmission. The important goal of molecular arithmetic can be achieved in principle "OFF-ON" digital AND, OR, NOT and XOR logic gates with independent inputs are available to operate on binary numbers.[57] Practical consideration would also require strong signals when these gates are in their "ON" states. Among the remaining logic gates are an inhibit function (INH) which can be interpreted as a particular integration of an AND and a NOT logic function, where the output signal is inhibited by one of the active inputs.[58]

Ligand **5b**, compound that undergoes a color change upon complexation, can be applied as an optical device. In this system, we know that ligand **5b** responds to cations or anion in a different way. On the basis of this strategy, we now demonstrate the properties of ligand **5b** that can be benefited as an INH gate.

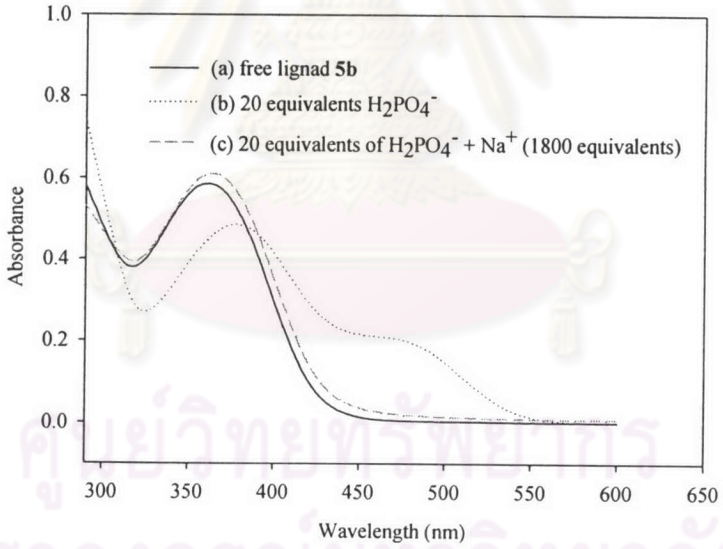

Figure 3.42 UV-vis spectrum of ligand **5b** in DMSO (2 X 10^{-5} M) (a) in its free form (b) in the presence of 20 equiv. of $H_2PO_4^-$ (c) in the presence of 20 equiv. of $H_2PO_4^-$ and 1800 equiv. of Na^+

Figure 3.42 shows the effect of the addition of $H_2PO_4^-$ and then an alkai metal ion (Na^+ or K^+) on the spectrum **5b** in DMSO (2 x 10^{-5} M). The maxima absorption with the nitrobenzene moieties of the ligand **5b** (λ = 361 nm, Figure 3.41a) clearly separates (λ = 459 nm) after addition of 20 equivalent of $H_2PO_4^-$ (as its

tetrabutylammonium salt). At the same time, a new absorbance appears at 459 nm (Figure 3.42b), resulting in a change in the appearance of the solution from yellow to deep red-orange. Interestingly, addition of an alkali metal ion (as perchlorate salt) reverses the chromogenic process. Upon addition of 1800 equivalents of an alkali metal ion to the solution (ClO_4^- does not complex with ligand **5b**), the deep red-orange color induced by the presence of $H_2PO_4^-$ was now no longer observable and the absorption maximum at 459 nm disappeared (Figure 3.42c).

For a comparison, the order of guest addition was then reversed. As expected, the addition of an alkali metal ion (1800 equivalents) to a solution of ligand **5b** in DMSO brought about no color change, although a small change in absorption intensity was observed. When 20 equivalents of $H_2PO_4^-$ were then added, the solution remained yellow and small changes in spectrum were observed. Therefore, an alkali metal ion appears to inhibit the chromogenic response of the system to $H_2PO_4^-$. A convenient way of representing these changes is through a molecular logic gate truth Table 3.5, which gives the logic response of ligand **5b** as 'ON' = 1 or 'OFF' = 0. In the presence of combinations of $H_2PO_4^-$ and an alkali metal ion at either 0 equivalent ('input' = 0) or 20 equivalents of $H_2PO_4^-$ and 1800 equivalents of alkali metal ion ('input' = 1). The output is only 1 if (anion, cation) = (1, 0). This logic response corresponds to the INH logic gate.

Table 3.7 The truth table of INH logic gate

INPUT		OUTPUT
$H_2PO_4^-$	alkali metal ion	color change
0	0	0
0	1	0
1	0	1
1	1	0

3.6 Electrochemical studies

Electrochemical techniques have been widely used as transduction methods for the conversion of chemical phenomena such as ion binding into electrical signals. This process is usually referred as electrochemical recognition. Nitrobenzene behaves as a chromophore and an electroactive functional group in a number of supramolecular systems.[59-62] It undergoes two reduction processes. The first process corresponds to a one-electron reduction and then follows by the second process to form a dianion according to the following equation. Nevertheless, very often the focus is on the first reduction process.[59,63]

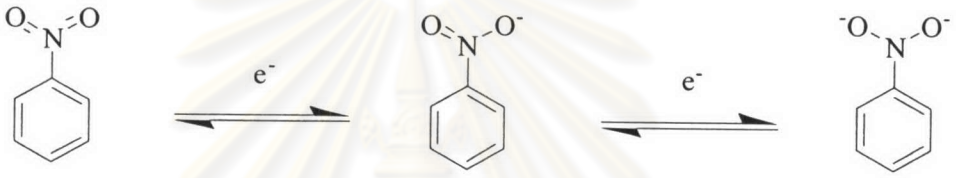

Thus, ligand **5b** has also been employed as an electrochemical receptor that possesses *p*-nitrophenyl moieties, electroactive functional groups. Herein, the aim of this section is to investigate the electroactivity of ligand **5b** in non-aqueous solvent and complexation of ligand **5b** with various ionic guests in connection with the possibility of electrochemical recognition.

3.6.1 Voltammograms of ligand 5b in DMF

Cyclic voltammograms of ligand **5b** in DMF with various scan rates are presented in Figure 3.43. They exhibit an irreversible first wave around E = -1418 mV due to two nitro-anion radicals with the presence of two nitro groups by a subsequent two electron transfer related to the cathodic peak that was assigned as I_C followed by a second wave at a much more negative potential with quasi-reversible wave at $E_{1/2}$ = -1825 mV that related to the cathodic wave (II_C). This is consistent with two electron reduction which leads to the formation of two nitro-dianions.

The peak current of the second reduction of ligand **5b** is linearly increasing by the square root of the scan rates in the range from 20 to 1000 mV (Figure 3.44), indicating that ligand **5b** follows only the diffusion controlled in the experimental condition.

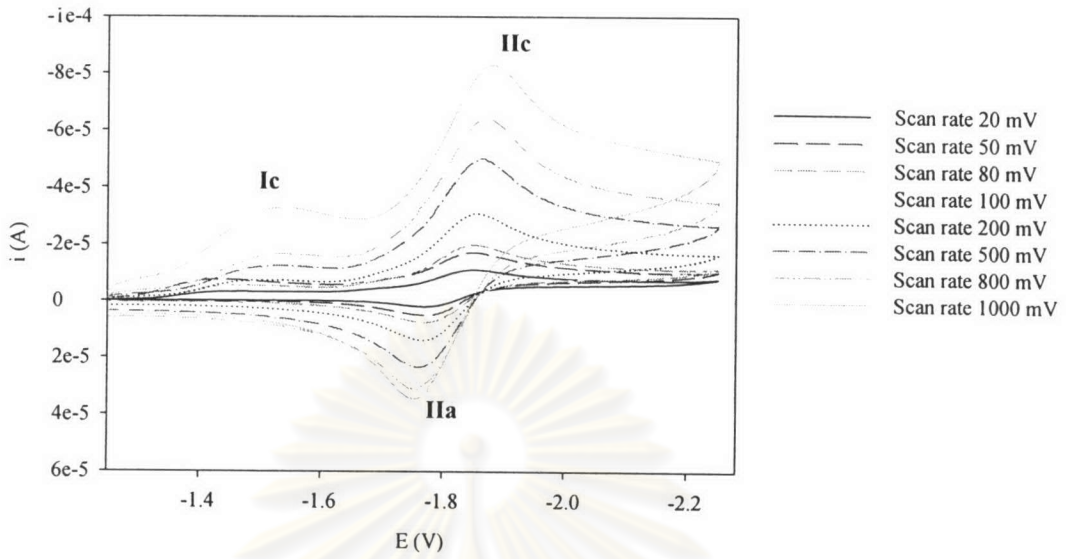

Figure 3.43 Cyclic voltammograms of ligand **5b** with various scan rates

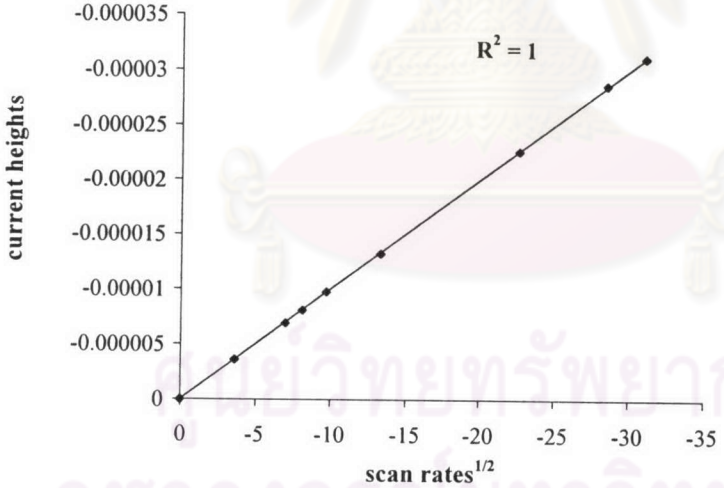

Figure 3.44 The plot between current heights of wave IIc and square root of scan rates

3.6.2 Electrochemical studies of ligand 5b with Na^+

When crown ether containing a nitrobenzene group as a side arm, was reduced to the corresponding anion radical and dianion, a new type of intramolecular cation complexes can be formed. Examples of such complexes have been reported to results from lariat ethers containing nitro aromatic residues. Indeed, the reduced ligands thus lead to excess negative charge which enhances the binding of cation more strongly than the corresponding neutral cases.

Based on our previous works of alkali metal ion complexation studies, we found that the glyme-5 moiety had selectivity towards Na^+. In this section, the electrochemical reduction of ligand **5b** in the presence of alkali metal ions is of interest, since it may provide a route to detect Na^+.

Upon addition of $NaClO_4$ to an electrochemical solution of ligand **5b**, Figure 3.45, a new irreversible (IIIc) wave at -2150 mV appears in voltammograms and shifts to anodic potential upon increasing the amount of $NaClO_4$. This wave shifts to -2010 mV while the quasi-reversible wave shifts slightly anodically to E = -1788 mV (related to IIc and IIa) and the initial irreversible wave (Ic) at -1412 V shifts insignificantly. Electrochemical data for the complex and free ligand **5b** are shown in Table 3.8. Squarewave voltammograms also support the results from cyclic voltammetry that not only a new peak gradually appears around -2150 mV and increases but also shifts slightly to positive potential at -2010 mV and less changes at the initial wave as shown in Figure 3.46.

We have two contingent explanations for the results; i) Na^+ probably mainly binds the tetraethylene glycol unit to form psuedocyclic crown ether ring and also interacts with the reduced nitro groups or, ii) Na^+ possibly interacts only with the reduced nitro groups due to Na^+ has a low binding ability toward the polyethylene glycol of ligand **5b**. Interestingly, the later case, supporting by the previous results, is more reasonable than the former case. Thus, the positive charge of Na^+ is stabilized by negative charge of the reduced nitro aromatic residues that drives the system to be reduced easily. Consequently, the quasi-reversible wave at -1822 mV slightly shifts to positive potential and the new irreversible wave appears at -2150 mV, which moves to anodic potential at -2050 mV when 4 equivalents of Na^+ are added. It may indicate that Na^+ forms a complex with the reduced form of ligand **5b** more stable than the neutral form that can utilizes for Na^+ ion analysis. Ligand **5b** may be applied to the fabrication of a molecular device that selectively recognizes Na^+.

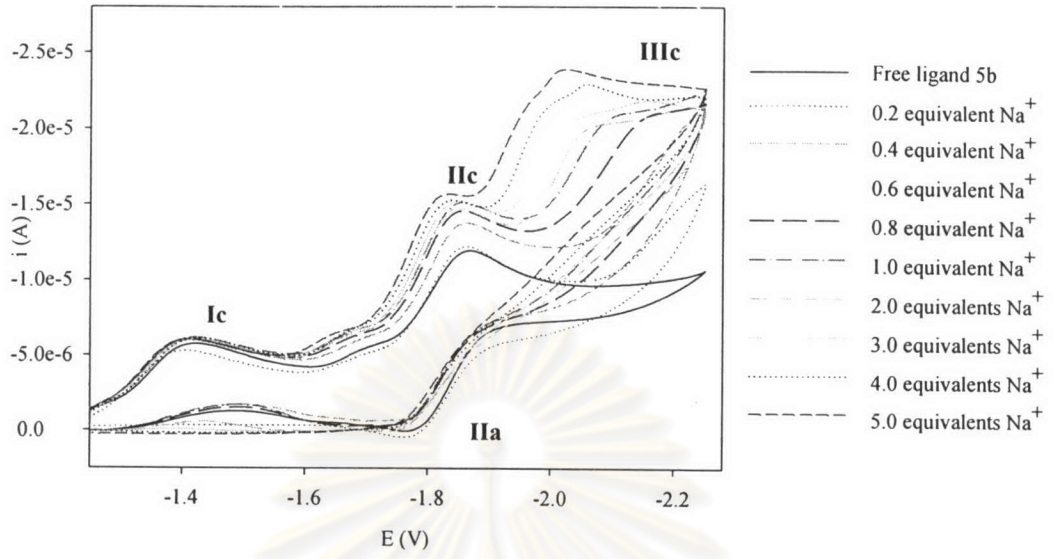

Figure 3.45 Cyclic voltammograms of ligand **5b** upon addition of Na^+

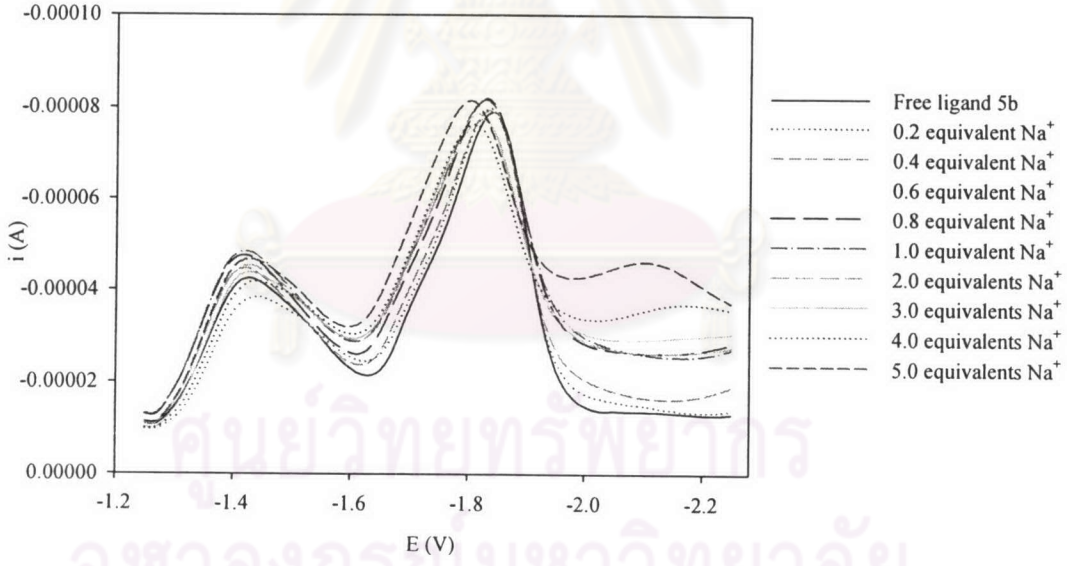

Figure 3.46 Square wave voltammograms of ligand **5b** upon addition of Na^+

Table 3.8 Electrochemical data of ligand **5b** and their complexes with Na^+

			mV				
equiv.	Ic	IIc	IIa	IIIc	EIIp	ΔEIc	ΔEIIp
0	-1412 (irr)	-1860 (q)	-1784 (q)	-	-1822	0	0
0.2	-1396 (irr)	-1854 (q)	-1781 (q)	-	-1818	-16	-4
0.4	-1396 (irr)	-1851 (q)	-1778 (q)	-	-1815	-16	-7
0.6	-1396 (irr)	-1851 (q)	-1775 (q)	-	-1813	-16	-9
0.8	-1396 (irr)	-1842 (q)	-1784 (q)	-2150 (irr)	-1813	-16	-9
1.0	-1396 (irr)	-1842 (q)	-1769 (q)	-2092 (irr)	-1806	-16	-16
1.5	-1393 (irr)	-1836 (q)	-1766 (q)	-2053 (irr)	-1801	-19	-21
2.0	-1393 (irr)	-1833 (q)	-1763 (q)	-2025 (irr)	-1800	-19	-22
3.0	-1393 (irr)	-1824 (q)	-1763 (q)	-2014 (irr)	-1794	-19	-28
4.0	-1393 (irr)	-1812 (q)	-1763 (q)	-2010 (irr)	-1788	-19	-34

3.6.3 Electrochemical studies of ligand 5b with various anions

Complexations between ligand **5b** and various anions were carried out in DMF using cyclic voltammetry with Bu_4PF_6 as supporting electrolyte for employing the electrochemical properties of complex behaviors. When an excess aliquot of Br^-, I^- and NO_3^- (4 equivalents) as their tetrabutylammonium salts was added to an electrolyte solution of ligand **5b**, cyclic voltammograms displayed no new wave and no noticeable peak shifts when compared with the original voltammogram of free ligand **5b**. For an example, Figure 3.47 exhibits cyclic voltammograms. The results were also supported by square wave voltammograms that were not drastically changes upon increasing the concentration of NO_3^- as shown in Figure 3.48. On the other hand, addition of Cl^- leaded to slightly cathodic shift relative to the wave Ic, while the initial wave at -1825 mV with respect to redox waves IIc and IIa did not change noticeably in their potential, Figure 3.49. This was consistent with square wave voltammograms, Figure 3.50 that confirmed the cathodic shift of the potential wave at -1418 mV upon increasing amount of Cl^-.

Conversely, on progressive addition of $H_2PO_4^-$ and BzO^- caused redox wave Ic shifted to a more negative potential than the original free ligand **5b** wave, meanwhile the quasi-reversible wave around -1821 mV shifted negligibly. Cyclic voltammograms are depicted in Figure 3.51 for $H_2PO_4^-$ and in Figure 3.53 for BzO^-. Square wave voltammograms clearly show the effect upon increasing the amount of $H_2PO_4^-$ (Figure 3.52) and BzO^- (Figure 3.54). In the presence of these anions, a new reduction peak grows and moves to more negative potential, at -1583 mV for $H_2PO_4^-$ and at -1558 mV for BzO^- concommitant with the decrease in the initial wave around -1821 mV. The results of electrochemical data between the complexes and free ligand **5b** are collected in Table 3.9. It should be noted that adding more than 2 equivalents of $H_2PO_4^-$ and BzO^- showed negligible changes of voltammograms. This implied in the 1:2 stoichiometry of the host:guest ratio as well as observed in the UV-vis titration technique.

On the other hand, the electrochemical solution of ligand **5b** was titrated with AcO^-, Figure 3.55. The redox peak Ic diminishes in its current height while a new redox peak IIc grows up and altogether shifts to more cathodic, finally reaching maximum value at -1598 mV by addition of 2 equivalents of AcO^-. Further addition of AcO^- did not significantly shifts the wave IIc. This signifies the formation of a 1:2 complex between ligand **5b** and AcO^-. However, increasing the amount of AcO^-

causes a redox wave at potential -1821 mV (related to peak IIIc and IIIa) shifts less positively and becomes an irreversible wave, (see Table 3.10). Square wave voltammograms (Figure 3.56) were also supported the electrochemical behavior of **5b**.AcO^- complex. Furthermore, addition of more than 2 equivalents of AcO^-, the current of the initial peak at -1821 mV not only gradually diminished but also shifted to slightly anodic potential and turned to a shoulder peak at -1803 mV, indicating a irreversible wave.

Upon analyzing the CV data from Tables 3.9 and 3.10, we observed that the difference of the cathodic shifts of the redox wave (Ic). These probably correlated with the qualitative stability constants for the anion complexes of the neutral form and rather influenced with a 1:2 than a 1:1 stoichiometry of the host:guest ratio as obtained by UV-vis titrations. We rationalized that strong anion complexes such as **5b**.$H_2PO_4^-$, **5b**.BzO^- and **5b**.AcO^-, binding in the 1:2 complexation, destabilized the reduced form of ligand **5b** as a consequence of the coulombic repulsion between the anions and the reduced nitro moieties of ligand **5b**. Moreover, the withdrawing electron density from the nitro aromatic residues by strong coordinated anions makes these systems more difficult to be reduced. Therefore, the cathodic wave Ic shifted more negative potential than that of free ligand **5b**. Additionally, a 1:2 complexation shifted more cathodically than a 1:1 complexation. In the 1:2 complexation, anions mainly associated on each thiourea and reduced electron density from the nitrophenyl residues over a 1:1 complexation, resulting in the less perturbation in electronic properties of the nitrophenyl residues.

ศูนย์วิทยทรัพยากร
จุฬาลงกรณ์มหาวิทยาลัย

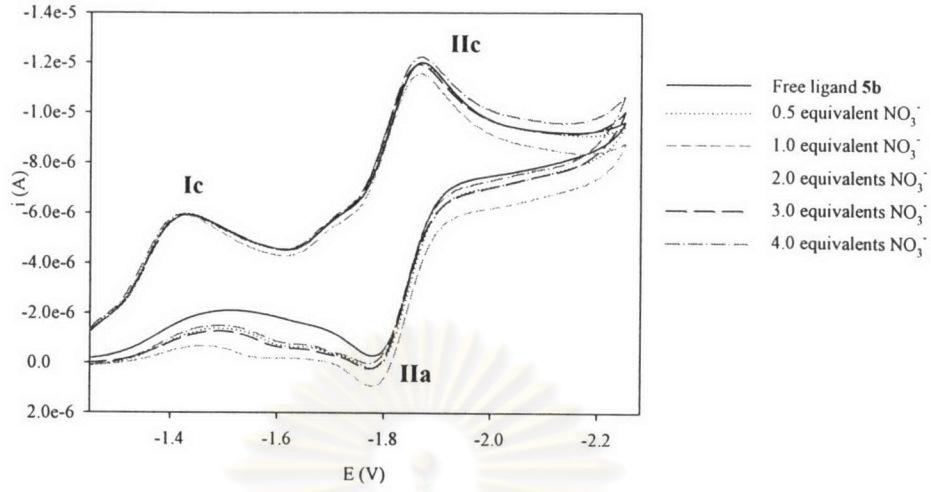

Figure 3.47 Cyclic voltammograms of ligand **5b** upon addition of NO_3^-

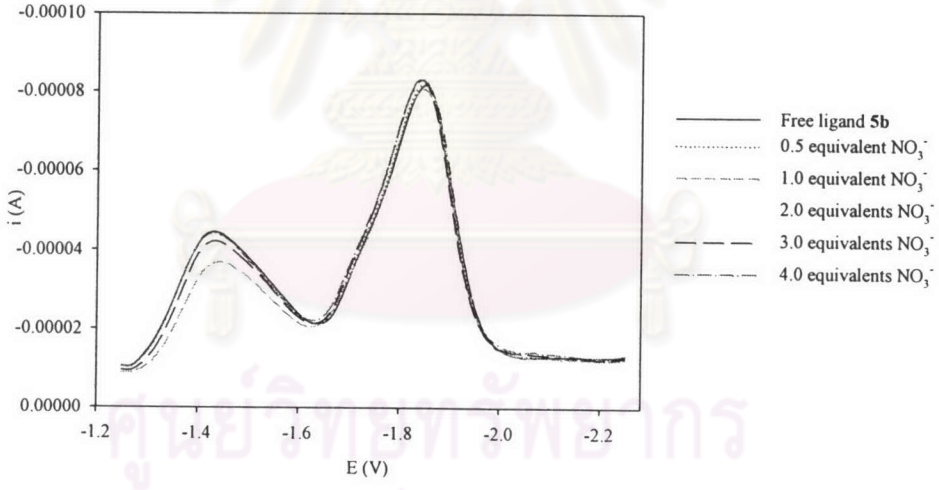

Figure 3.48 Square wave voltammograms of ligand **5b** upon addition of NO_3^-

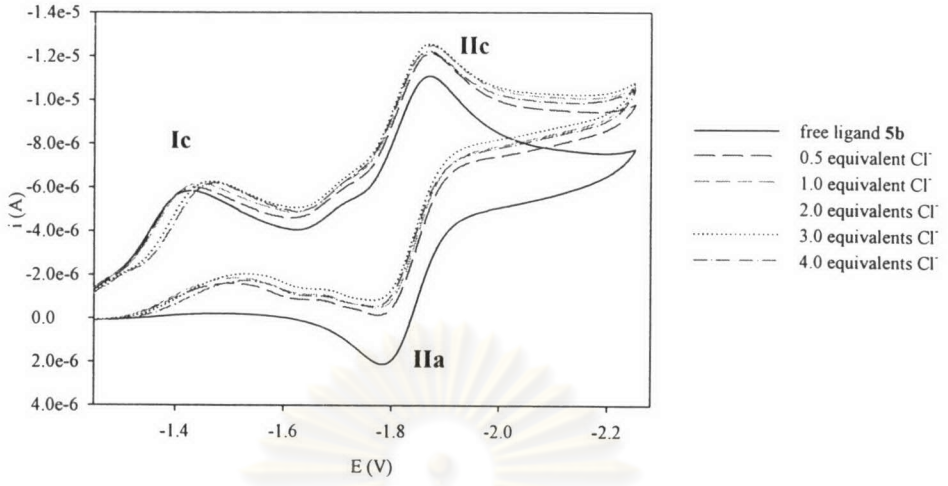

Figure 3.49 Cyclic voltammograms of ligand **5b** upon addition of Cl^-

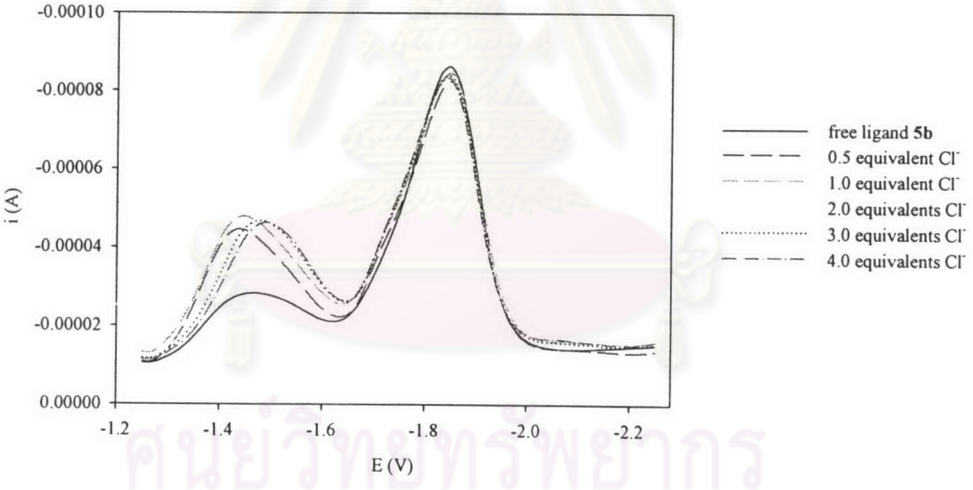

Figure 3.50 Square wave voltammograms of ligand **5b** upon addition of Cl^-

ศูนย์วิทยทรัพยากร
จุฬาลงกรณ์มหาวิทยาลัย

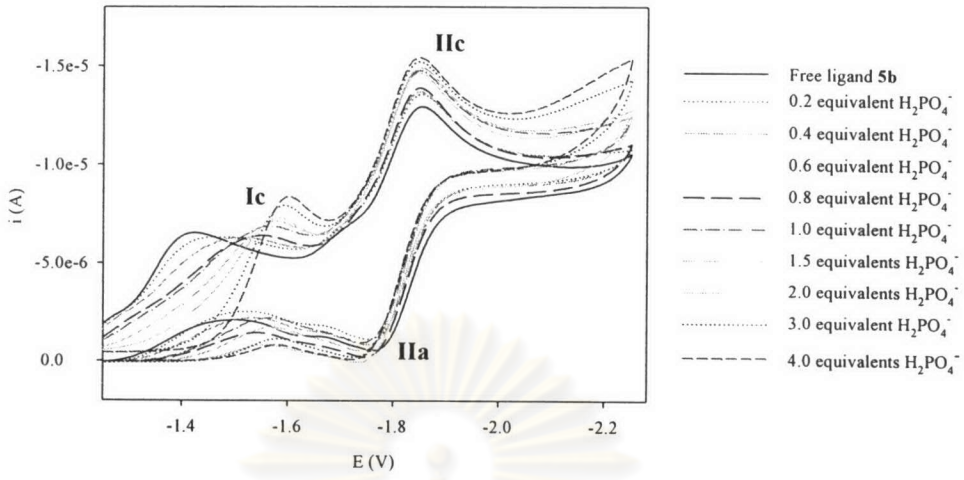

Figure 3.51 Cyclic voltammograms of ligand **5b** upon addition of $H_2PO_4^-$

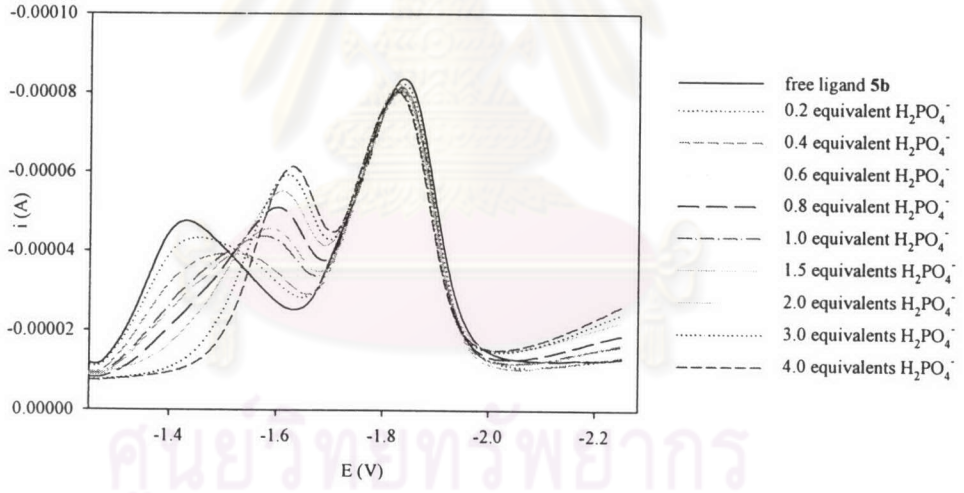

Figure 3.52 Square wave voltammograms of ligand **5b** upon addition of $H_2PO_4^-$

ศูนย์วิทยทรัพยากร
จุฬาลงกรณ์มหาวิทยาลัย

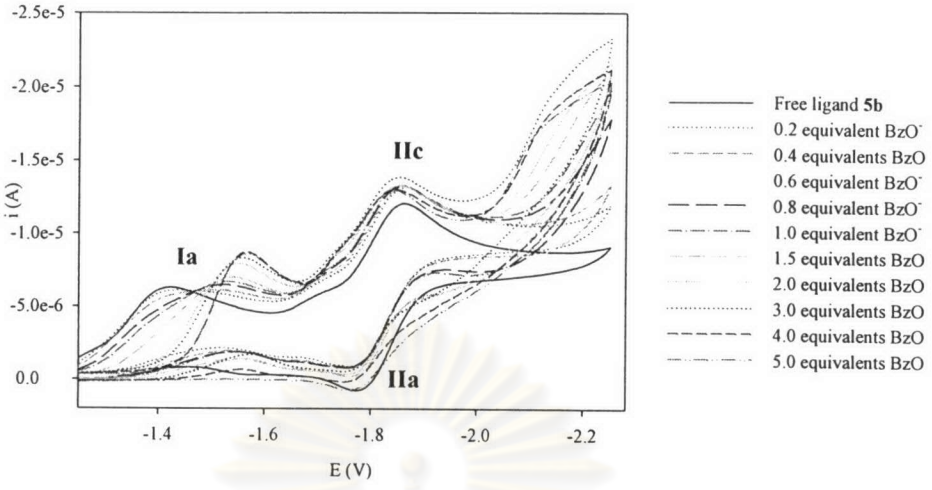

Figure 3.53 Cyclic voltammograms of ligand **5b** upon addition of BzO^-

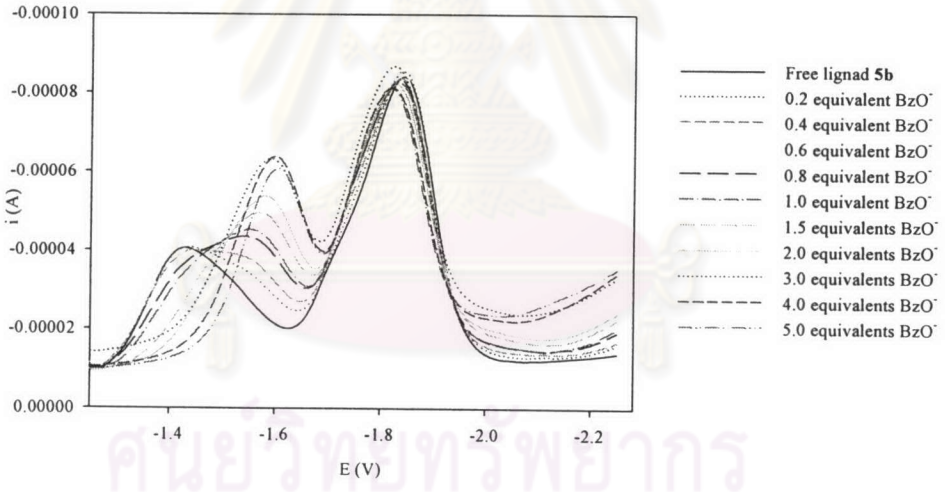

Figure 3.54 Square wave voltammograms of ligand **5b** upon addition of BzO^-

ศูนย์วิทยทรัพยากร
จุฬาลงกรณ์มหาวิทยาลัย

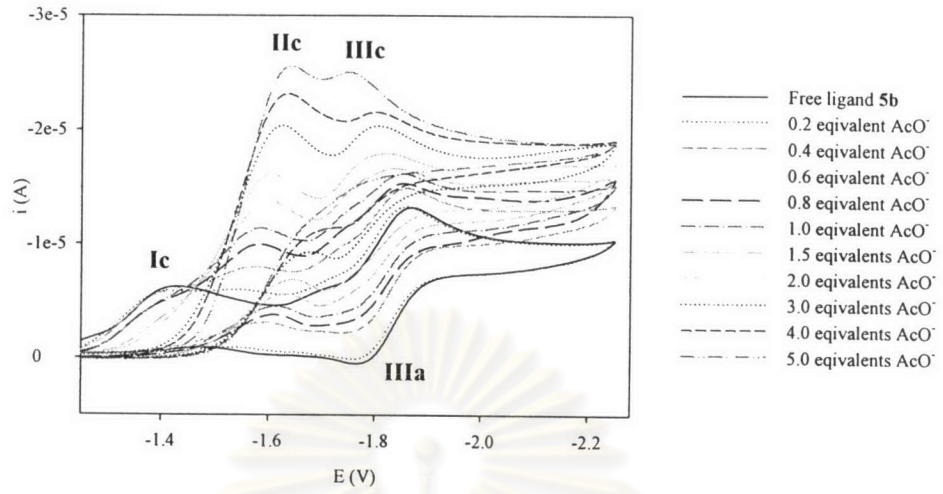

Figure 3.55 Cyclic voltammograms of ligand **5b** upon addition of AcO^-

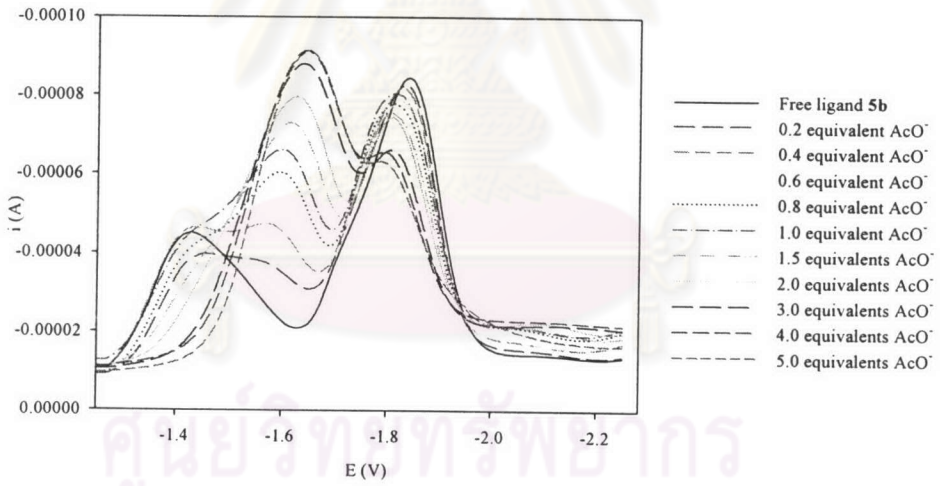

Figure 3.56 Square wave voltammograms of ligand **5b** upon addition of AcO^-

Table 3.9 Electrochemical data of ligand **5b** and their complexes with anionic guests

anion	equivalents	Ic	IIc	IIa	EIIp	ΔEIIp	ΔEIc
				mV			
Cl^-	0	-1418 (irr)	-1863 (q)	-1787 (q)	-1825	0	0
	0.5	-1424 (irr)	-1863 (q)	-1787 (q)	-1825	0	6
	1.0	-1430 (irr)	-1863 (q)	-1787 (q)	-1825	0	12
	2.0	-1454 (irr)	-1863 (q)	-1787 (q)	-1825	0	36
	3.0	-1454 (irr)	-1863 (q)	-1787 (q)	-1825	0	36
	4.0	-1458 (irr)	-1860 (q)	-1787 (q)	-1824	-1	40
Br^-	0	-1412 (irr)	-1860 (q)	-1784 (q)	-1822	0	0
	0.2	-1412 (irr)	-1860 (q)	-1784 (q)	-1822	0	0
	0.4	-1412 (irr)	-1860 (q)	-1784 (q)	-1822	0	0
	0.6	-1413 (irr)	-1860 (q)	-1784 (q)	-1822	0	1
	0.8	-1413 (irr)	-1860 (q)	-1784 (q)	-1822	0	1
	1.0	-1419 (irr)	-1860 (q)	-1784 (q)	-1822	0	7
	1.5	-1419 (irr)	-1860 (q)	-1784 (q)	-1822	0	7
	2.0	-1419 (irr)	-1854 (q)	-1781 (q)	-1818	-4	7
	3.0	-1419 (irr)	-1854 (q)	-1781 (q)	-1818	-4	7
	4.0	-1419 (irr)	-1854 (q)	-1781 (q)	-1818	-4	7

Table 3.9 Electrochemical data of ligand **5b** and their complexes with anionic guests (continued)

anion	equivalents	Ic	IIc	IIa	Ep	ΔEIIp	ΔEIc
				mV			
I^-	0	-1412 (irr)	-1866 (q)	-1790 (q)	-1828	0	0
	0.5	-1415 (irr)	-1866 (q)	-1790 (q)	-1828	0	3
	1.0	-1415 (irr)	-1866 (q)	-1787 (q)	-1827	-1	3
	2.0	-1418 (irr)	-1863 (q)	-1787 (q)	-1825	-3	6
	3.0	-1421 (irr)	-1863 (q)	-1787 (q)	-1825	-3	9
	4.0	-1421 (irr)	-1863 (q)	-1787 (q)	-1825	-3	9
NO_3^-	0	-1418 (irr)	-1863 (q)	-1787 (q)	-1825	0	0
	0.5	-1418 (irr)	-1863 (q)	-1787 (q)	-1825	0	0
	1.0	-1418 (irr)	-1863 (q)	-1787 (q)	-1825	0	0
	2.0	-1421 (irr)	-1863 (q)	-1787 (q)	-1825	0	3
	3.0	-1421 (irr)	-1863 (q)	-1787 (q)	-1825	0	3
	4.0	-1421 (irr)	-1863 (q)	-1787 (q)	-1825	0	3
$H_2PO_4^-$	0	-1409 (irr)	-1848 (q)	-1778 (q)	-1813	0	0
	0.2	-1424 (irr)	-1848 (q)	-1775 (q)	-1812	-1	15
	0.4	-1485 (irr)	-1845 (q)	-1769 (q)	-1807	-6	76
	0.6	-1509 (irr)	-1845 (q)	-1763 (q)	-1804	-9	100
	0.8	-1528 (irr)	-1845 (q)	-1763 (q)	-1804	-9	119

Table 3.9 Electrochemical data of ligand **5b** and their complexes with anionic guests (continued)

				mV			
Anion	equivalents	Ic	IIc	IIa	Ep	ΔEIIp	ΔEIc
$H_2PO_4^-$	1.0	-1549 (irr)	-1845 (q)	-1763 (q)	-1804	-9	140
	1.5	-1561 (irr)	-1845 (q)	-1757 (q)	-1801	-12	152
	2.0	-1570 (irr)	-1842 (q)	-1757 (q)	-1800	-13	161
	3.0	-1580 (irr)	-1842 (q)	-1750 (q)	-1796	-17	171
	4.0	-1583 (irr)	-1852 (q)	-1750 (q)	-1801	-12	174
BzO^-	0	-1412 (irr)	-1857 (q)	-1784 (q)	-1821	0	0
	0.2	-1415 (irr)	-1857 (q)	-1784 (q)	-1821	0	3
	0.4	-1470 (irr)	-1854 (q)	-1775 (q)	-1815	-6	58
	0.6	-1497 (irr)	-1854 (q)	-1772 (q)	-1813	-8	85
	0.8	-1516 (irr)	-1851 (q)	-1769 (q)	-1810	-11	104
	1.0	-1522 (irr)	-1851 (q)	-1772 (q)	-1812	-9	110
	1.5	-1531 (irr)	-1848 (q)	-1775 (q)	-1812	-9	119
	2.0	-1543 (irr)	-1845 (q)	-1772 (q)	-1809	-12	131
	3.0	-1549 (irr)	-1842 (q)	-1769 (q)	-1806	-15	137
	4.0	-1551 (irr)	-1839 (q)	-1769 (q)	-1804	-17	139

Table 3.10 Electrochemical data of ligand **5b** and its complex with AcO^-

		mV						
anion	equivalents	Ic	IIc	IIIc	IIIa	EIIIp	ΔEIIIp	ΔEIc*
AcO^-	0	-1415 (irr)	-	-1860 (q)	-1781 (q)	-1821	0	0
	0.2	-1418 (irr)	-1552 (irr)	-1854 (q)	-1778 (q)	-1816	-5	137
	0.4	-1420 (irr)	-1561 (irr)	-1854 (q)	-1760 (q)	-1807	-14	146
	0.6	-1424 (irr)	-1567 (irr)	-1851 (q)	-1760 (q)	-1806	-15	152
	0.8	-1431 (irr)	-1573 (irr)	-1845 (q)	-1760 (q)	-1803	-18	158
	1.0	-	-1573 (irr)	-1845 (q)	-1754 (q)	-1800	-21	158
	1.5	-	-1592 (irr)	-1827 (q)	-1714 (q)	-1771	-50	177
	2.0	-	-1598 (irr)	-1805 (q)	-1714 (q)	-1760	-61	183
	3.0	-	-1619 (irr)	-1805 (q)	-1732 (q)	-1769	-52	204
	4.0	-	-1628 (irr)	-1805 (q)	-1766 (q)	-1786	-35	213
	5.0	-	-1635 (irr)	-1763 (irr)	-	-	-	220

* The cathodic shifts of the redox wave Ic (ΔEIc) are relative to the wave IIIc

3.6.4 Electrochemical studies of ligand 5b in the presence of 2 equivalents of $NaClO_4$ toward chosen anions such as $H_2PO_4^-$, AcO^- and BzO^-

In this section, we have focused on examination of the electrochemical behaviors and binding abilities of complexes between Na^+ with ligand **5b** toward chosen anions, such as $H_2PO_4^-$, BzO^- and AcO^-, which exhibited remarkable changes in electrochemical properties. Furthermore, we expected to obtain advanced information for supporting the evidence of ion pairing effect. CV titration experiments were carried out repeatedly in the presence of 2 equivalents of $NaClO_4$ with Bu_4NPF_6 as a supporting electrolyte.

Results from the titration between **5b**.Na^+ and $H_2PO_4^-$ are presented in Figure 3.57 and electrochemical data are listed in Table 3.11. Increasing equivalents of $H_2PO_4^-$ causes drastically cathodic shift relative to the redox wave Ic concommitant with the disappearance of the initial wave IIIc, representing in complexation of Na^+ with the reduced nitro residues, and negligible changes in quasi-reversible (related to peak IIc and IIa) are observed. Further addition of one more equivalents of $H_2PO_4^-$ leads to completely disappear of the redox wave IIIc. Voltammograms seem to be the same as the system in the presence of only excess $H_2PO_4^-$. Square wave voltammograms clearly show peak shifts of the initial wave Ic (E = -1409 mV) concommitant with the disappearance of the initial wave (IIIc) at E = -2031 mV as shown in Figure 3.58.

Upon addition of BzO^-, the initial reversible wave (IIIc) at -2001 mV gradually disappears in voltammograms (Figure 3.59) and slightly shifts to positive potential while the irreversible wave (Ic) at -1403 mV displays remarkable cathodic shift and quasi reversible at -1784 mV shifts insignificantly. Adding more than 2 equivalents of BzO^- produced votammograms similar to the system in the presence of only excess BzO^-. Square wave voltammograms (Figure 3.60) are in good agreement with cyclic voltammograms.

Addition of AcO^- resulted in the original redox wave Ic at -1406 mV and IVc at -2047 mV diminishes in their current height and shifts more cathodically concommitant with the growth of the new wave IIc that shifts to negative potential at -1641 mV. In addition, increasing equivalent of AcO^- more than 2 equivalents causes the quasi reversible wave (related to IIIc and IIIa) becomes irreversible wave while the irreversible wave IVc completely disappears, which generated voltammograms similar to the systems of adding only excess AcO^- as shown in Figure 3.61. The

elecreochemical data of the titration between **5b**.Na^+ and AcO^- are given in Table 3.12. Square wave voltammograms, Figure 3.62, also support the CV results that exhibit substantial shifts to cathodic potential relative to wave Ic which accompany to the growth of the wave at -1614 mV. Furthermore, addition of AcO^- over 2 equivalents, the current of the initial peak at -1815 mV not only gradually diminishes but also shifts more anodically and becomes a shoulder peak at -1760 mV which is similar to the system of adding only excess AcO^-.

According to the electrochemical behaviors and data in Tables 3.11 and 3.12, in all cases, we observed two significant characteristic results: i) the initial wave around -2000 mV, indicating interactions between Na^+ and the reduced nitro residues, shifted cathodically and completely dispeared upon increasing amount of such anions that showed clearly in the case of **5b**.$Na^+/H_2PO_4^-$. ii) The redox wave Ic in all cases exhibited drastic shifts to negative potential. Apparently, two notable changes upon addition of the chosen anions to the electrochemical solution of ligand **5b** in the presence of 2 equivalents of $NaClO_4$ induced voltammograms which seem to be identical shifts of peak Ic and exactly the same as voltammograms in the system with adding of only excess anion.

The bifunctinal ligand **5b** in neutral form has efficient abilities to bind such anions stronger over Na^+. Although, even the reduced form of ligand **5b** probably coordinates Na^+ stronger and more stable than the neutral form. Adddition of such anions to the electrochemical solution is assumed that anions bind tightly with thiourea moieties and some bound Na^+, which has low binding ability toward ligand **5b**, to form ion-pairing species that diminish the electron withdrawing property of Na^+. Unfortunately, upon applying the potential to the system; strongly coordinated anion by nitro-thiourea residues and ion pairing effect cause this electrochemical system to be hardly reduced in the nitrophenyl moieties. Further supporting of the ion pair formation implied by the instant vanishing of wave IIIc after addition a few equivalents of $H_2PO_4^-$ and suddenly remarkable shifts of wave Ic after addition of more than 2 equivalents. We suggest that the beginning equivalent of $H_2PO_4^-$ principally operates with Na^+ to form ion paring. Until reaching 2 equivalents, ion paring probably forms completely. Further addition, $H_2PO_4^-$ is mainly coordinated to the nitro residues causing in significant shifts of the wave Ic.

Conversely, in the cases of AcO^- and BzO^-, the reduction wave Ic gradually shifts and the potential wave around -2000 mV disappears. Hence, these anions

probably incorporate to Na^+ as well as to the nitro urea moieties resulting in lower ion pairing formation when compare to the case of $H_2PO_4^-$, that plays a crucial role to bind Na^+. We believe that $Na^+/H_2PO_4^-$ has the possibility to form ion pairing over Na^+/BzO^- and Na^+/AcO^-, corresponding in the cooperativity factors (Figure 3.38) as described above. Unfortunately, in the case of Na^+/AcO^-, we have no sufficient and good evidence for more comparison and discussion with both cases of $Na^+/H_2PO_4^-$ and Na^+/BzO^-. Nevertheless, this assumption should be investigated further for obtaining more supporting results.

In conclusion, the probable failure of Na^+ binding ability in this system was attributed to the ion pairing effect. The high ability of anion complexation resulted in the nitro residues to be less reducible.

ศูนย์วิทยทรัพยากร
จุฬาลงกรณ์มหาวิทยาลัย

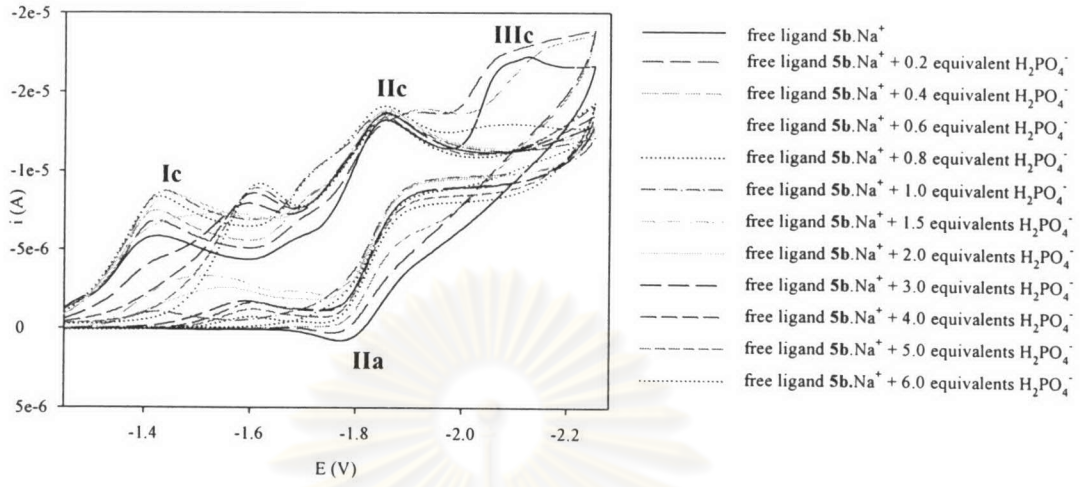

Figure 3.57 Cyclic voltammograms of ligand **5b.**Na^+ upon addition of $H_2PO_4^-$

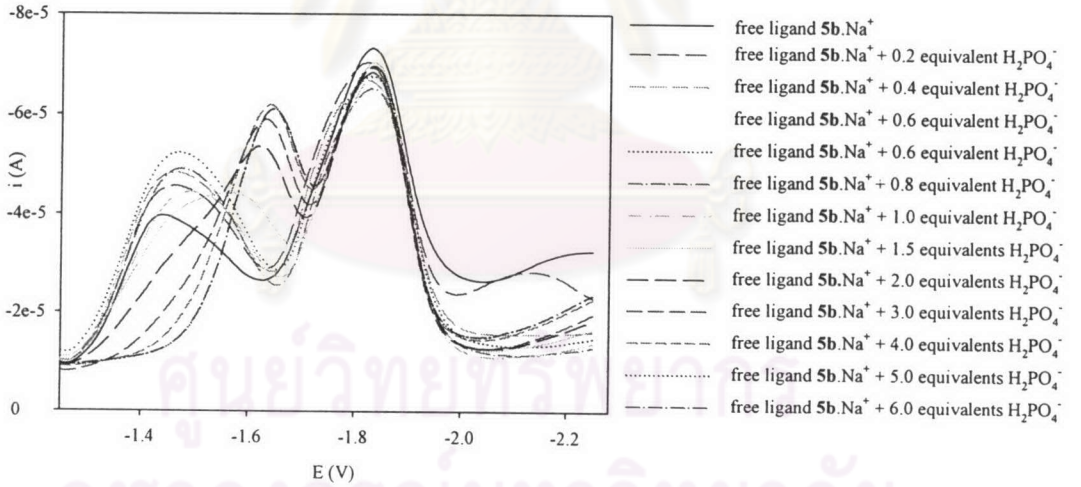

Figure 3.58 Square wave voltammograms of ligand **5b.**Na^+ upon addition of $H_2PO_4^-$

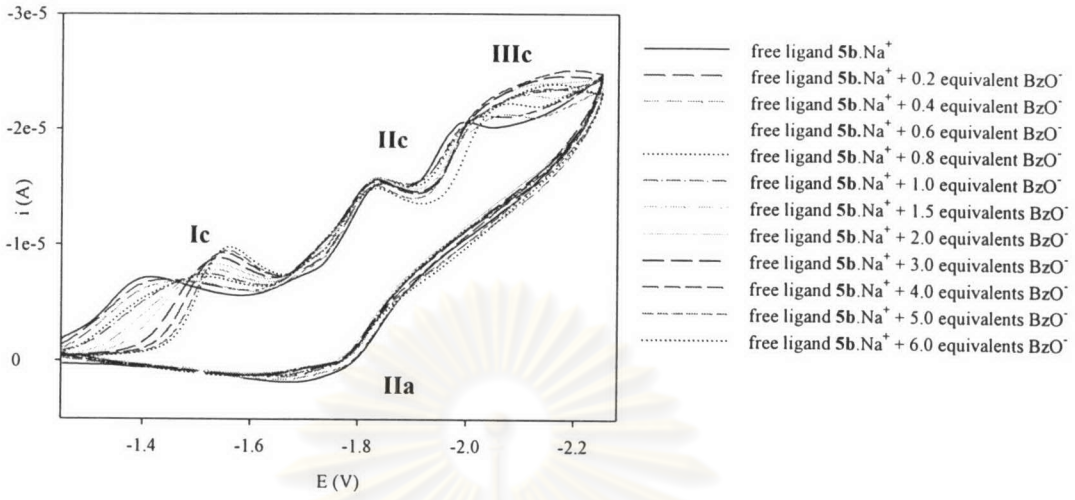

Figure 3.59 Cyclic voltammograms of ligand **5b**.Na^+ upon addition of BzO^-

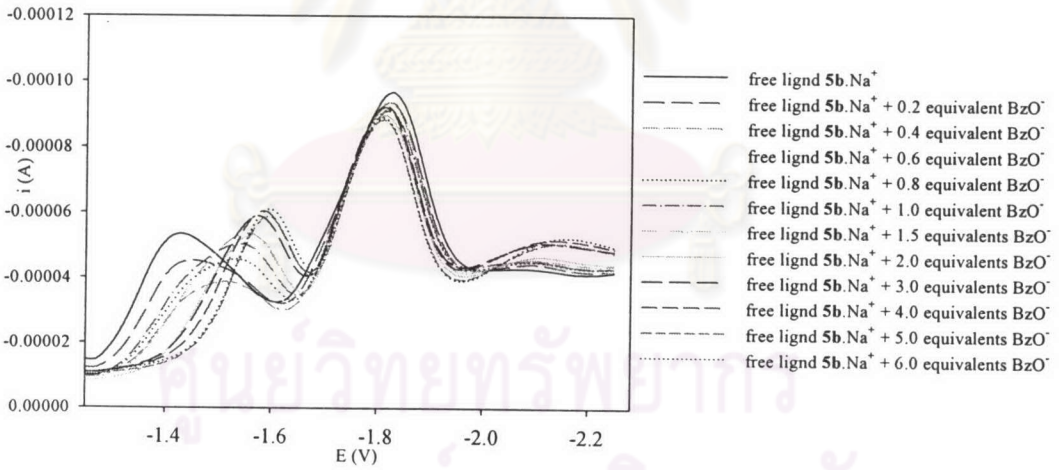

Figure 3.60 Square wave voltammograms of ligand **5b**.Na^+ upon addition of BzO^-

ศูนย์วิทยทรัพยากร
จุฬาลงกรณ์มหาวิทยาลัย

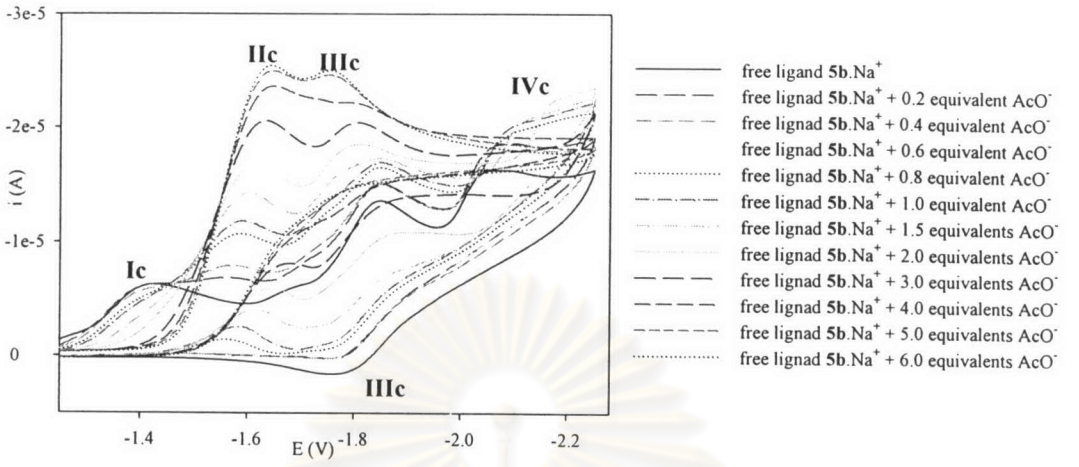

Figure 3.61 Cyclic voltammograms of ligand **5b.**Na^+ upon addition of AcO^-

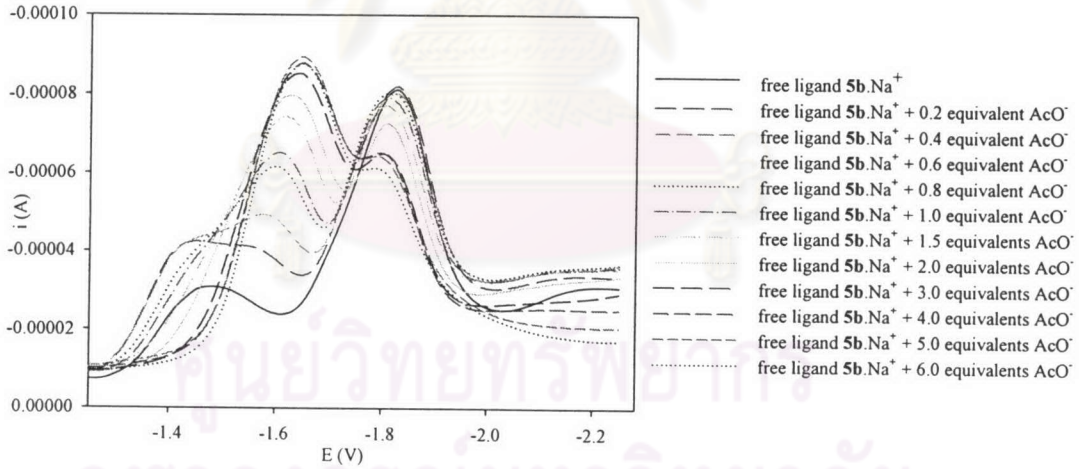

Figure 3.62 Square wave voltammograms of ligand **5b.**Na^+ upon addition of AcO^-

ศูนย์วิทยทรัพยากร
จุฬาลงกรณ์มหาวิทยาลัย

Table 3.11 Electrochemical data of ligand **5b**.Na^+ and their complexes with anionic guests

		mV						
anion	equivalents	Ic	IIc	IIa	EIIp	IIIc	ΔEIIp	ΔEIc
$H_2PO_4^-$	0	-1409 (irr)	-1842 (q)	-1787 (q)	-1815	-2031 (irr)	0	0
	0.2	-1415 (irr)	-1844 (q)	-1784 (q)	-1814	-2031 (irr)	-1	6
	0.4	-1415 (irr)	-1845 (q)	-1784 (q)	-1815	small	0	6
	0.6	-1418 (irr)	-1845 (q)	-1784 (q)	-1815	small	0	9
	0.8	-1424 (irr)	-1848 (q)	-1781 (q)	-1815	-	0	15
	1.0	-1433 (irr)	-1851 (q)	-1772 (q)	-1812	-	-3	24
	1.5	-1445 (irr)	-1854 (q)	-1766 (q)	-1810	-	-5	36
	2.0	-1454 (irr)	-1854 (q)	-1766 (q)	-1810	-	-5	45
	3.0	-1583 (irr)	-1854 (q)	-1766 (q)	-1810	-	-5	174
	4.0	-1595 (irr)	-1854 (q)	-1763 (q)	-1810	-	-5	186
	5.0	-1604 (irr)	-1854 (q)	-1763 (q)	-1809	-	-6	195
	6.0	-1607 (irr)	-1854 (q)	-1763 (q)	-1809	-	-6	198

Table 3.11 Electrochemical data of ligand **5b.**Na^+ and their complexes with anionic guests (coninued)

				mV				
anion	equivalents	Ic	IIc	IIa	EIIp	IIIc	ΔEIIp	ΔEIc
BzO^-	0	-1403 (irr)	-1833 (q)	-1784 (q)	-1809	-2001 (irr)	0	0
	0.2	-1418 (irr)	-1827 (q)	-1781 (q)	-1804	-2007 (irr)	-5	15
	0.4	-1436 (irr)	-1827 (q)	-1775 (q)	-1801	-2034 (irr)	-8	33
	0.6	-1464 (irr)	-1824 (q)	-1775 (q)	-1800	-2040 (irr)	-9	61
	0.8	-1500 (irr)	-1824 (q)	-1775 (q)	-1800	-2053 (irr)	-9	97
	1.0	-1509 (irr)	-1824 (q)	-1775 (q)	-1800	-	-9	106
	1.5	-1516 (irr)	-1824 (q)	-1772 (q)	-1798	-	-11	113
	2.0	-1525 (irr)	-1824 (q)	-1772 (q)	-1798	-	-11	122
	3.0	-1534 (irr)	-1824 (q)	-1772 (q)	-1798	-	-11	131
	4.0	-1540 (irr)	-1824 (q)	-1772 (q)	-1798	-	-11	137
	5.0	-1549 (irr)	-1824 (q)	-1772 (q)	-1798	-	-11	146
	6.0	-1552 (irr)	-1824 (q)	-1769 (q)	-1797	-	-12	149

Table 3.12 Electrochemical data of ligand **5b**.Na^+ and its complex with AcO^-

anion	equivalents	mV Ic	IIc	IIIc	IIIa	EIIIp	IVc	ΔEIIp	ΔEIc*
AcO^-	0	-1406 (irr)	-	-1842 (q)	-1787 (q)	-1815	-2047 (irr)	0	0
	0.2	-1406 (irr)	-1558 (irr)	-1842 (q)	-1787 (q)	-1815	-2059 (irr)	0	152
	0.4	-1406 (irr)	-1564 (irr)	-1842 (q)	-1787 (q)	-1815	-2062 (irr)	0	158
	0.6	small	-1573 (irr)	-1842 (q)	-1779 (q)	-1811	-2080 (irr)	-4	167
	0.8	small	-1577 (irr)	-1842 (q)	-1776 (q)	-1809	-2081 (irr)	-6	171
	1.0	small	-1580 (irr)	-1842 (q)	-1754 (q)	-1798	-2083 (irr)	-17	174
	1.5	-	-1595 (irr)	-1836 (q)	-1741 (q)	-1789	-2114 (irr)	-26	189
	2.0	-	-1610 (irr)	-1796 (q)	-1741 (q)	-1769	-2169 (irr)	-46	204
	3.0	-	-1628 (irr)	-1802 (q)	-1723 (q)	-1763	-	-52	222
	4.0	-	-1638 (irr)	-1808 (q)	-1738 (q)	-1773	-	-42	232
	5.0	-	-1641 (irr)	-1763 (q)	-	-	-	-	235
	6.0	-	-1641 (irr)	-1760 (q)	-	-	-	-	235

* The cathodic shifts of the redox wave Ic (ΔEIc) are relative to the wave IIIc

3.6.5 Electrochemical studies of ligand 5b in the presence of an chosen anions such as $H_2PO_4^-$, AcO^- and BzO^- toward Na^+

In the final section, the electrochemical behaviors of their anion complexation of ligand **5b** with Na^+ were examined in order to evaluate the influence of the anion complexation which possibly discovers the evidence of ion pairing. The CV titration between Na^+ and the electrochemical solution of ligand **5b** in the presence of 2 equivalents of $H_2PO_4^-$ changes cyclic voltammograms (Figure 3.63) in the following ways. Addition of the 1 equivalent of Na^+, the initial wave Ic at -1586 mV and the quasi reversible wave at potential -1812 mV (related to IIc and IIa) shifted insignificantly. As increasing Na^+ more than 1 equivalent, the single irreversible wave Ic splitted into two peaks and depleted in its current height (see Table 3.13) altogether with the growth of a new splitted irreversible wave IIIc, that intermediately shifted to more positive potential. Interestingly, upon addition of 4 equivalents of Na^+, a new anodic wave IVc at -1625 mV appeared. On progressive addition, it moved to merge the initial wave IIa, generating a broad redox wave IIc. Therefore, EIIp could not be determined accurately. Addition of excess Na^+ caused anodic shift of wave Ic that returned to the potential around -1412 mV as the same potential of the redox wave Ic of free ligand **5b**. In addition, we did not observe the redox wave around -2000 mV in these voltammograms, representing in the interaction between Na^+ and the reduced nitro groups. Consequently, the occurring voltammograms seem to be quite identical to that of free ligand **5b**. Square wave voltammograms were in a good accordance with cyclic voltammograms that clearly showed the completely anodic reversion of wave Ic to its original potential as shown in Figure 3.64.

In the case of BzO^-, addition of Na^+ into this system altered cyclic voltammograms as shown in Figure 3.65, the initial wave Ic shifted fairly to positive potential while the quasi reversible wave with respect to waves IIc and IIa shifted less anodically. After reaching 1 equivalent of Na^+, a newly irreversible wave IIIc at -2050 mV evolved concommitant with anodic shifts of its potential. Interestingly, the anodic shifts and the occurring redox wave IIIc were changed instantly remarkable during addition of 2 equivalents of Na^+. At higher 3 equivalents of Na^+, the current height of the initial wave IIa depleted while a newly anodic wave IVa around -1595 mV, a small irreversible wave, appeared during addition of 5 equivalents of Na^+ (see Table 3.14). Square wave voltammogroms also supported to the results of cyclic voltammograms that not only the new wave IIIc gradually appeared at more negative

potential around -1961 mV and grew up but also the initial Ic completely vanished as shown in Figure 3.66.

On the other hand, the electrochemical solution of **5b**.AcO^- was titrated with Na^+. Cyclic voltammograms, Figure 3.67, exhibited a similar fashion as the case of **5b**.BzO^-. Increasing the equivalents of Na^+ caused the initial cathodic wave Ic slightly shifted to positive potential and quasi reversible (related to IIc and IIa) shifted fairly to more anodic potential. After reaching 1.5 equivalents of Na^+, a newly irreversible redox wave IIIc appeared at more negative potential around -2190 mV altogether with the continually anodic shifts of its potential. Apparently, upon addition of 3 equivalents of Na^+, the occurring redox wave IIIc displayed remarkable changes in its potential (see Table 3.15). Addition of excess Na^+ (5 equivalents) exhibited negligible changed in cyclic voltammograms. Square wave voltammograms, Figure 3.68, were in good agreement with the results of cyclic voltammograms that show clearly the gradual appearance of the new redox wave IIIc around -2022 mV.

Inspection of the electrochemical results, we think that ion pairing effects also occurred in these systems. In order to confirm these phenomena, we gave the first attention to the case of $H_2PO_4^-$ that absolutely illustrates important evidences. Before applying potential to this electrochemical system, we presume that added Na^+ is principally bound with coordinated anions by the nitro thiourea moieties to form ion pair that diminishes electron density from $H_2PO_4^-$. Thus, after applying potential to this system, a consequence of the diminishing electron density of $H_2PO_4^-$ by the ion pair formation makes the nitro aromatic residues be reduced more easily. This evidence is in good agreement with the voltammograms that exhibit gradually anodic shifts of the redox wave Ic and not be found redox wave around -2000 mV, representing in the interaction between Na^+ and the reduced nitro groups, due to no available Na^+ to interact with the reduced nitro groups. Consequently, entire amount of Na^+ is mainly form ion pair with coordinated $H_2PO_4^-$. Interestingly, the anodic shift of the initial wave Ic relative to the splitting wave IIIc (see Table 3.13) change remarkably during addition of 2 equivalents of Na^+. On progressive addition, voltammograms change insignificantly. Hence, coordinated anions with nitro thiourea moieties are probably dissociated from their binding sites by forming ion pair with Na^+ outside the cavity, which forms completely upon reaching 2 equivalents of Na^+. However, Addition of higher equivalents of Na^+ causes the anodic shift of the initial wave Ic that absolutely returns to its original potential of the system of free ligand

5b, regarding to the wave IIIc around -1412 mV in this system. Furthermore, the appearing voltammograms seem to be nearly the voltammogram of free ligand **5b**. This implies that no anions bound to the nitro thiourea moieties due to a high efficiency of ion pairing ability of $Na^+/H_2PO_4^-$.

Similarly, in the case of AcO^- and BzO^-, the existing results are well established that ion pairing plays a crucial in this system. In additional details, the initial wave Ic in both cases of AcO^- and BzO^- shifts less anodically and is not completely reversible to its original potential when compare to the case of $H_2PO_4^-$. This probably suggest that the ion pairing ability of Na^+/BzO^- and Na^+/AcO^- are lower than $Na^+/H_2PO_4^-$, which support our assumption in the previous section. Moreover, a consequence of low ion pairing ability, we postulate that Na^+ behaves as co-bound anions to form ion pair that does not dissociate from the coordinated anions.

More importantly, unlike the case of $H_2PO_4^-$, the occurring redox wave IIIc with respect to the interaction between Na^+ and the reduced nitro residues is observed by addition of 1-1.5 equivalents of Na^+ and exhibited immediately remarkable shifts to anodic potential during addition 3 equivalents of Na^+. Base on our assumption, these phenomena imply that the majority of Na^+ principally incorporated with coordinated anions to form ion pair and the less interaction with the reduced nitro residues. Nevertheless, reaching 2 equivalents of Na^+, ion paring may occur completely. Therefore, at higher 3 equivalents of Na^+, excess Na^+ mainly coordinates to the reduce nitro residues, causing the anodic shift of the redox wave IIIc.

Finally, all results in this section support our previous assumption (in section 3.6.5) and lead to conclude that ion pairing effect plays an important role in this system due to the low binding ability of Na^+ toward the neutral form of ligand **5b**.

ศูนย์วิทยทรัพยากร
จุฬาลงกรณ์มหาวิทยาลัย

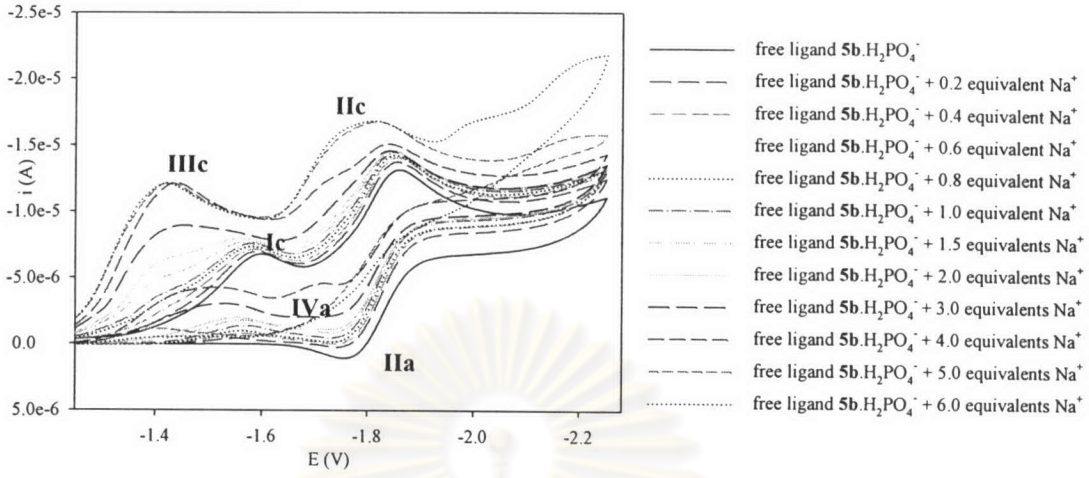

Figure 3.63 Cyclic voltammograms of ligand **5b**.$H_2PO_4^-$ upon addition of Na^+

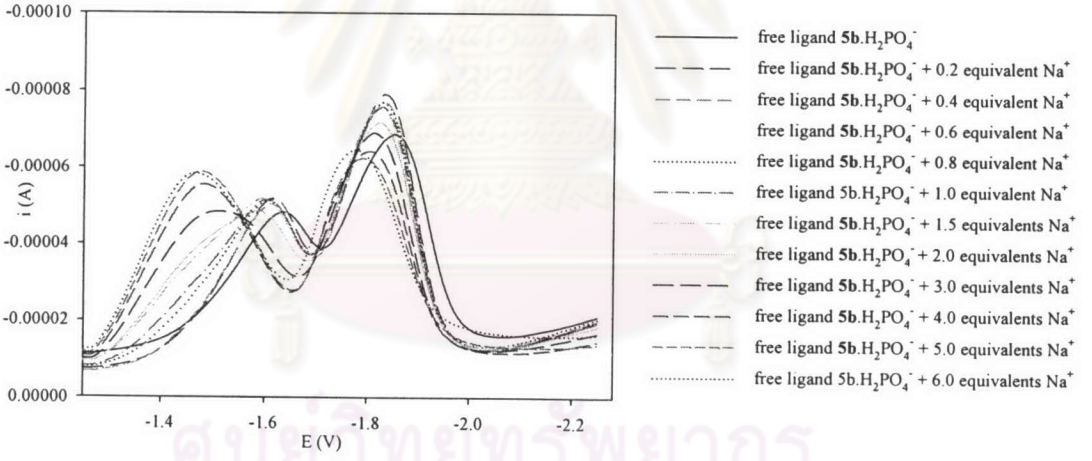

Figure 3.64 Square wave voltammograms of ligand **5b**.$H_2PO_4^-$ upon addition of Na^+

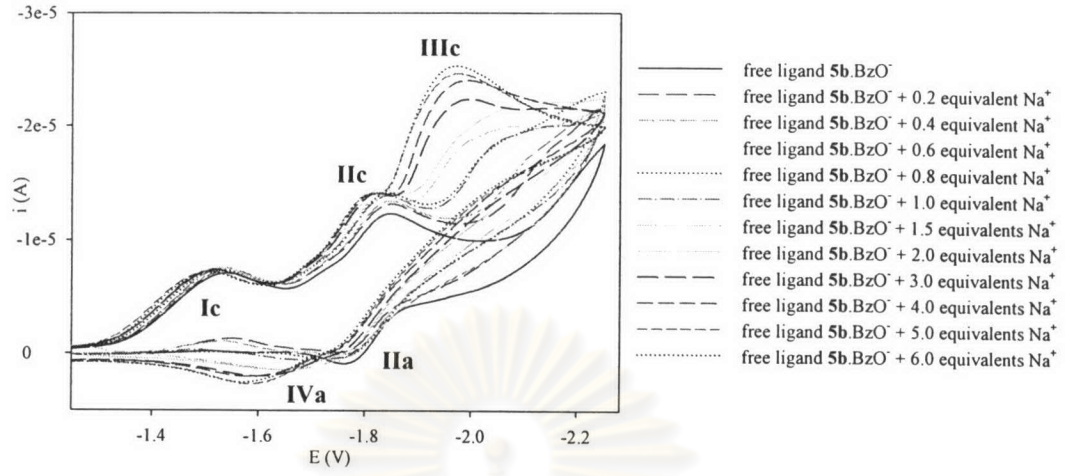

Figure 3.65 Cyclic voltammograms of ligand **5b**.BzO$^-$ upon addition of Na^+

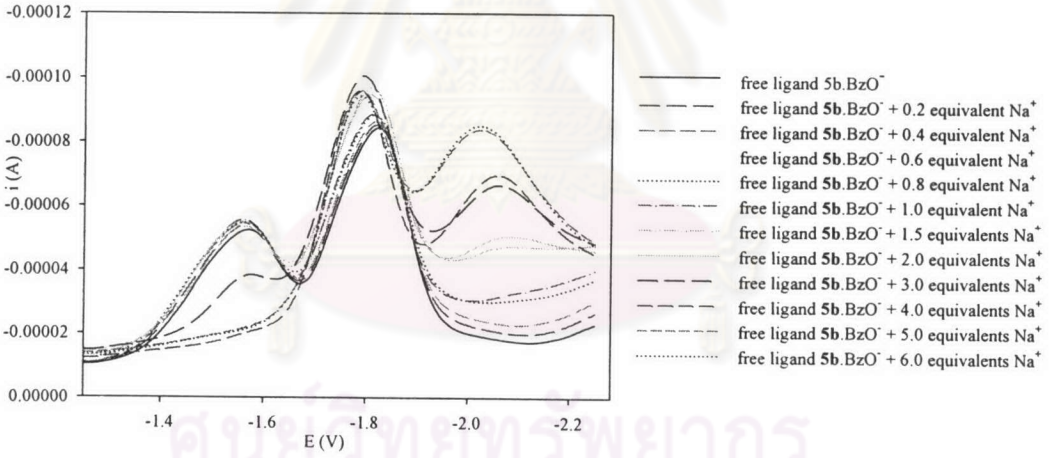

Figure 3.66 Square wave voltammograms of ligand **5b**.BzO$^-$ upon addition of Na^+

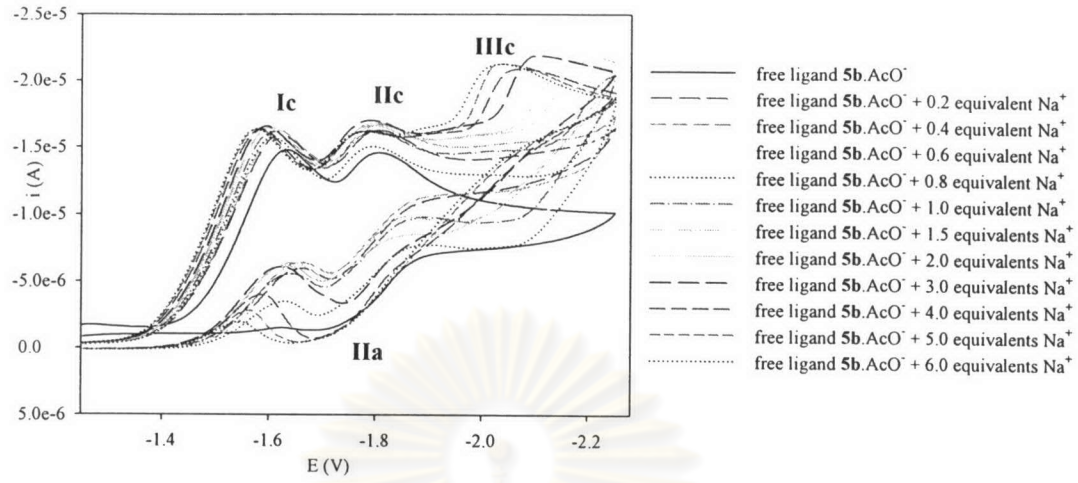

Figure 3.68 Square wave voltammograms of ligand **5b**.AcO$^-$ upon addition of Na$^+$

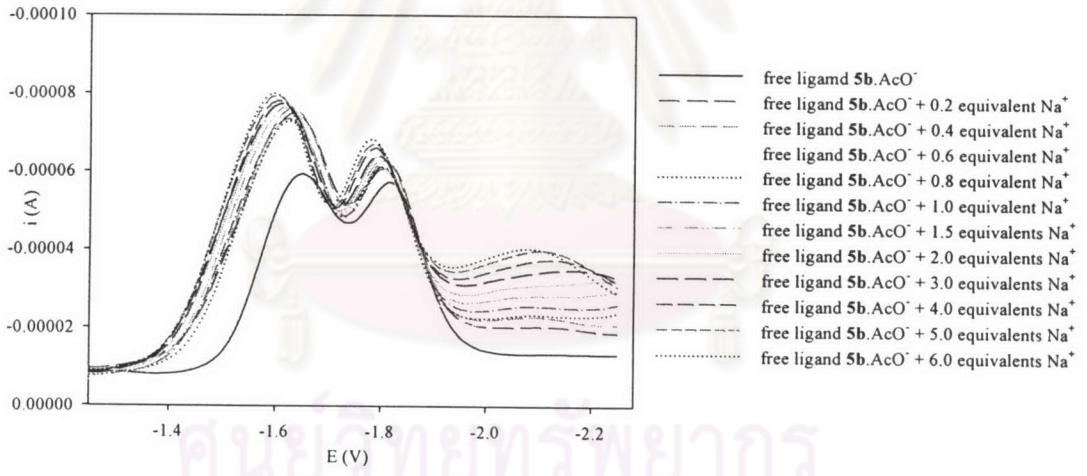

Figure 3.67 Cyclic voltammograms of ligand **5b**.AcO$^-$ upon addition of Na$^+$

ศูนย์วิทยทรัพยากร
จุฬาลงกรณ์มหาวิทยาลัย

Table 3.13 Electrochemical data of ligand **5b**.$H_2PO_4^-$ and its complex with Na^+

	mV							
equivalents	Ic	IIc	IIa	IIIc	IVa	EIIp	ΔEIIp	ΔEIc*
0	-1586 (irr)	-1854 (q)	-1769 (q)	-	-	-1812	0	0
0.2	-1580 (irr)	-1854 (q)	-1763 (q)	-	-	-1809	-3	-6
0.4	-1577 (irr)	-1848 (q)	-1754 (q)	-	-	-1801	-11	-9
0.6	-1570 (irr)	-1848 (q)	-1754 (q)	-	-	-1801	-11	-9
0.8	-1570 (irr)	-1848 (q)	-1754 (q)	-	-	-1801	-11	-16
1.0	-1561 (irr)	-1848 (q)	-1754 (q)	-	-	-1801	-11	-16
1.5	-1555 (irr)	-1845 (q)	-1754 (q)	-1391(small, irr)	-	-1800	-12	-25
2.0	-	-1842 (q)	-1754 (q)	-1396 (irr)	-	-1798	-14	-190
3.0	-	-1839 (q)	-1754 (q)	-1437 (irr)	-	-1797	15	-149
4.0	-	-1839 (q)	-1754 (q)	-1460 (irr)	-1625 (irr)	-1797	-15	-156
5.0	-	-1815 (q)	-1683 (br, q)	-1421 (irr)	-	-1749	-63	-165
6.0	-	-1802 (q)	-1705 (br, q)	-1412 (irr)	-	-1754	-58	-174

* The cathodic shifts of the redox wave Ic (ΔEIc) are relative to the wave IIIc

Table 3.14 Electrochemical data of ligand **5b**.BzO^- and its complex with Na^+

	mV								
equivalents	Ic	IIc	IIa	IIIc	IVa	EIIp	ΔEIIp	ΔEIc	ΔEIIIc
0	-1534 (irr)	-1845 (q)	-1778 (q)	-	-	-1812	0	0	-
0.2	-1531 (irr)	-1845 (q)	-1775 (q)	-	-	-1810	-2	-3	-
0.4	-1528 (irr)	-1842 (q)	-1775 (q)	-	-	-1809	-3	-6	-
0.6	-1519 (irr)	-1836 (q)	-1775 (q)	-	-	-1806	-6	-15	-
0.8	-1516 (irr)	-1836 (q)	-1775 (q)	-	-	-1806	-6	-18	-
1.0	-1516 (irr)	-1836 (q)	-1772 (q)	-2050 (irr)	-	-1803	-9	-18	0
1.5	-1516 (irr)	-1833 (q)	-1769 (q)	-2010 (irr)	-	-1795	-17	-18	-40
2.0	-1509 (irr)	-1821 (q)	-1763 (q)	-2004 (irr)	-	-1792	-20	-25	-16
3.0	-1506 (irr)	-1805 (q)	-1760 (q)	-1970 (irr)	-	-1783	-29	-28	-80
4.0	-1503 (irr)	-1805 (q)	-1760 (q)	-1967 (irr)	-	-1783	-29	-31	-83
5.0	-1488 (irr)	-1790 (q)	-1760 (q)	-1961 (irr)	-1595 (irr)	-1775	-37	-46	-89
6.0	-1488 (irr)	-1790 (q)	-1760 (q)	-1961 (irr)	-1595 (irr)	-1775	-37	-46	-89

Table 3.15 Electrochemical data of ligand **5b**.AcO^- and its complex with Na^+

	mV							
equivalents	Ic	IIc	IIa	IIIc	EIIp	ΔEIIp	ΔEIc*	ΔEIIIc
0	-1628 (irr)	-1805 (q)	-1732 (q)	-	-1769	0	0	-
0.2	-1616 (irr)	-1802 (q)	-1729 (q)	-	-1766	-3	-12	-
0.4	-1613 (irr)	-1799 (q)	-1720 (q)	-	-1760	-9	-15	-
0.6	-1604 (irr)	-1793 (q)	-1720 (q)	-	-1757	-12	-24	-
0.8	-1607 (irr)	-1790 (q)	-1720 (q)	-	-1755	-14	-21	-
1.0	-1601 (irr)	-1787 (q)	-1711 (q)	-	-1749	-20	-27	-
1.5	-1598 (irr)	-1787 (q)	-1717 (q)	-2190 (irr)	-1752	-17	-30	0
2.0	-1592 (irr)	-1784 (q)	-1711 (q)	-2156 (irr)	-1748	-21	-36	-34
3.0	-1589 (irr)	-1778 (q)	-1744 (q)	-2089 (irr)	-1761	-8	-39	-101
4.0	-1580 (irr)	-1769 (q)	-1696 (q)	-2056 (irr)	-1733	-36	-48	-134
5.0	-1573 (irr)	-1763 (q)	-1686 (q)	-2028 (irr)	-1725	-44	-55	-162
6.0	-1570 (irr)	-1757 (q)	-1680 (q)	-2022 (irr)	-1719	-50	-58	-168